The Stimulated Raman Threshold II: Theory

Francis F. Chen

PPG-893 Sept. 1985

Electrical Engineering Department
School of Engineering and Applied Science
University of California, Los Angeles 90024

The stimulated Raman threshold II: Theory

Francis F. Chen

Electrical Engineering Department, University of California, Los Angeles
California 90024

(Received)

Experimental results on the stimulated Raman scattering threshold covering a large parameter range are compared with theory and are found to be in disagreement in most cases. Retaining the group velocity of the plasma waves yields a theoretical threshold lower than previously obtained.

I. INTRODUCTION

Though the conditions for excitation of the stimulated Raman scattering (SRS) instability have been given by numerous authors, observations of SRS have repeatedly been reported to occur when the threshold conditions are not met. We have confirmed this in our own experiment, reported in the companion paper (I). In this paper we first review the experimental evidence for agreement or disagreement of the SRS threshold with theory by using a simple model with which all experiments can be compared on the same basis. We then propose, in the second half of the paper, a way in which theoretical thresholds can be lowered to agree better with experiment.

Because of the sensitivity of the plasma wave dispersion relation to density variations, it was pointed out long ago[1] that the SRS threshold is dominated by the plasma inhomogeneity. To calculate the threshold accurately, however, requires a knowledge of the density profile and, except for simple profiles, a numerical calculation for each case. It has therefore been suggested[2] that a sufficiently accurate approximation is that of a homogeneous plasma of finite length L, where L is the maximum distance over which the excitation can occur resonantly in a real plasma because of phase slippage. Specifically, L can be identified as the distance between WKB turning points in the inhomogeneous-plasma problem. The finite-length SRS threshold has also been computed by a number of authors[3]. This bounded-plasma model is the one we adopt.

Some non-physical effects may appear if the interaction region has sharply defined boundaries. Reflections from the ends can give rise to positive feedback, causing a convective instability to become absolute. The boundaries can be effectively softened by changing the profile of the pump wave amplitude. Indeed, when this is done, it is found[4] that the distinction between convective

and absolute instability is obscured, or at least more difficult to generalize. We are therefore careful to consider only those effects that have a physical basis, and not those arising solely from the mathematical model. We also neglect pump depletion in view of the small SRS reflectivities found in experiment.

II. THEORY OF SRS IN A FINITE INTERACTION REGION

We review the well known formulation of this problem primarily for the purpose of establishing the notation. Let the plasma inhomogeneity, if any, lie in the x direction, and let the pump (0), plasma (1), and reflected (2) waves have the form

$$\underline{E}_o = \hat{y}\, E_o \cos(k_o x - \omega_o t) \tag{1}$$

$$n_1 = n_1(x,t)\sin(k_1 x - \omega_1 t) \tag{2}$$

$$E_2 = \hat{y}\, E_2(x,t)\cos(k_2 x - \omega_2 t), \tag{3}$$

where $n_1(x,t)$ and $E_2(x,t)$ are slowly varying amplitudes, and E_o is taken to be constant. Assume that the waves (ω_o, k_o), (ω_1, k_1), and (ω_2, k_2) obey both their respective linear dispersion relations and the phase matching conditions $\omega_o = \omega_1 + \omega_2$ and $k_o = k_1 + k_2$. Standard analysis[5,6] then yields these coupled equations for the amplitudes n_1 and E_2:

$$\frac{\partial n_1}{\partial t} + \frac{3v_e^2 k_1}{\omega_1}\frac{\partial n_1}{\partial x} + \gamma_1 n_1 = a_1 E_2 \tag{4}$$

$$\frac{\partial E_2}{\partial t} + \frac{c^2 k_2}{\omega_2}\frac{\partial E_2}{\partial x} + \gamma_2 E_2 = a_2 n_1 \ , \tag{5}$$

where γ_1, γ_2 are the phenomenological damping rates of n_1 and E_2, respectively, and the coupling coefficients a_1, a_2 are given by

$$a_1 = (\omega_p^2 k_1^2 / m\omega_o \omega_1 \omega_2)(E_o/16\pi) \quad (6)$$

$$a_2 = \pi e^2 E_o / m\omega_o \quad . \quad (7)$$

For definiteness, we chose $\underline{k}_o$ to be in the $-\hat{x}$ direction, so that $\underline{k}_1$ and $\underline{k}_2$ are in the $-\hat{x}$ and $+\hat{x}$ directions, respectively, for direct backscatter. The group velocity magnitudes are then given by

$$V_1 = -3v_e^2 k_1/\omega_1 \quad (8)$$

$$V_2 = c^2 k_2/\omega_2 \simeq c \quad . \quad (9)$$

The homogeneous growth rate γ_o is found by neglecting the $\gamma_{1,2}$ and $V_{1,2}$ terms; then

$$\gamma_o^2 = a_1 a_2 = \frac{k_1^2}{16}\left(\frac{eE_o}{m\omega_o}\right)^2 \frac{\omega_p^2}{\omega_1\omega_2} \simeq \frac{1}{4}\frac{v_o^2}{c^2}\omega_o\omega_p \quad . \quad (10)$$

The last equality results from the definition $v_o = eE_o/m\omega_o$ and the low-n_o, T_e approximations $k_1 \simeq 2k_o$, $\omega_2 \simeq \omega_o$, and $\omega_1^2 = \omega_p^2 + 3k_1^2 v_e^2 \simeq \omega_p^2$.
It is convenient to use γ_o^2 as a measure of pump intensity I_o, where $I_o(W/cm^2) = cE_o^2/8\pi \times 10^7$. For $\lambda_o = 2\pi c/\omega_o$ in μm, we obtain

$$I_o = 2905\ \gamma_o^2/\lambda_o\omega_p \quad (I_o \text{ in } W/cm^2,\ \lambda_o \text{ in } \mu m) \quad . \quad (11)$$

Steady-state solutions of Eqs. (4) and (5) are given by

$$-V_1 n' + \gamma_1 n_1 = a_1 E_2 \tag{12}$$

$$V_2 E'_2 + \gamma_2 E_2 = a_2 n_1 \, . \tag{13}$$

Defining $$\kappa_1 = \gamma_1/V_1 \, , \quad \bar{a}_1 = a_1/V_1 \tag{14}$$

$$\kappa_2 = \gamma_2/V_2 \, , \quad \bar{a}_2 = a_2/V_2 \tag{15}$$

$$\kappa_o^2 = \bar{a}_1 \bar{a}_2 = \gamma_o^2/V_1 V_2 \, , \tag{16}$$

we now have

$$-n'_1 + \kappa_1 n_1 = \bar{a}_1 E_2 \tag{17}$$

$$E'_2 + \kappa_2 E_2 = \bar{a}_2 n_1 \, , \tag{18}$$

where κ_1, κ_2 are the spatial damping rates of the plasma and backscattered waves. Since $\gamma_2 < \gamma_1$ and $V_2 >> V_1$, we generally have $\kappa_1 >> \kappa_2$.

If ω_p is constant, we can differentiate Eq. (17) and combine with Eqs. (18) and (16) to obtain

$$n''_1 - (\kappa_1 - \kappa_2) n'_1 + (\kappa_o^2 - \kappa_1 \kappa_2) n_1 = 0 \, . \tag{19}$$

E_2 obeys the same equation. Fourier components $n_1 \simeq n_1 \exp(\kappa x)$ obey the condition

$$\kappa^2 - \kappa(\kappa_1 - \kappa_2) + (\kappa_o^2 - \kappa_1 \kappa_2) = 0 \, . \tag{20}$$

The homogeneous threshold κ_h is defined by setting $\kappa = 0$:

$$\kappa_o^2 = \kappa_1 \kappa_2 \equiv \kappa_h^2 \, , \quad \gamma_h^2 \equiv \gamma_1 \gamma_2 = \kappa_h^2 V_1 V_2 \, . \tag{21}$$

The solutions to Eq. (20) are given by

$$\kappa = \frac{1}{2}(\kappa_1 - \kappa_2) \pm \left[\frac{1}{4}(\kappa_1 + \kappa_2)^2 - \kappa_o^2\right]^{\frac{1}{2}} \quad . \tag{22}$$

Waves growing exponentially in space are thus possible if

$$\kappa_o^2 < \frac{1}{4}(\kappa_1 + \kappa_2)^2 \equiv \kappa_a^2 \quad , \tag{23}$$

which yields the usual expression for the "absolute" thrshold for densities below quarter-critical:

$$\gamma_a^2 = \frac{1}{4}\left(\frac{\gamma_1}{V_1} + \frac{\gamma_2}{V_2}\right)^2 V_1 V_2 \quad . \tag{24}$$

Thus, if $\gamma_o < \gamma_a$, κ is real and the space dependence is exponential; if $\gamma_o > \gamma_a$, κ is complex, and the space dependence is sinusoidal. However, in the sinusoidal case this steady-state solution, as will be apparent in Sec. IV, becomes infinite for certain values of L, and therefore the time dependence cannot be negleeted. For $\gamma_o < \gamma_a$, the steady-state solution is the fastest growing mode in space, and hence is important in inhomogeneous or bounded plasmas. To see this, use the Laplace transform and replace the time derivatives in Eqs. (4) and (5) by γn_1 and γE_2, respectively. Then κ_1 and κ_2 become $\kappa_1 = (\gamma + \gamma_1)/V_1$ and $\kappa_2 = (\gamma + \gamma_2)/V_2$. Since $\kappa \propto 1/\kappa_1$ (see below), the largest κ is for $\gamma = 0$.

The customary solution for the $\gamma_o < \gamma_a$ case is found by neglecting the term $-V_1 n_1'$ in Eq. (12) because the plasma wave group velocity V_1 is comparatively small. This is tantamount to dropping the κ^2 term in Eq. (20), and the solution is

$$\kappa = \frac{\kappa_o^2 - \kappa_1\kappa_2}{\kappa_1 - \kappa_2} \simeq \frac{\kappa_o^2}{\kappa_1} \simeq \frac{\gamma_o^2}{c\gamma_1} \quad . \tag{25}$$

This familiar formula assumes that $\gamma_o >> \gamma_h$, $\kappa_1 >> \kappa_2$, and $V_2 \simeq c$. Since $E_2 = (\kappa_1/\bar{a}_1)n_1$ in this case, both n_1 and E_2 grow from noise at the rate $\exp(\kappa x)$. Thus if the interaction region is from x = 0 to x = L and the noise levels are $n_1^o = n_1(0)$ and $E_2^o = E_2(0)$, the backscatter power is proportional to

$$E_2^2(L) = (E_2^o)^2 \, e^{2N} \quad , \quad N = \kappa L = \gamma_o^2 L/c\gamma_1 \quad . \tag{26}$$

When $\gamma_o \gtrsim \gamma_a$, no simple solution exists; one must compute the growth of wave packets, as has been done in several papers[7-9]. In this case, the sensitivity to the assumed initial conditions is not easily studied.

When $\gamma_o >> \gamma_a$, dissipation can be neglected, and one has the classical convective instability[1]. Eq. (22) becomes

$$\kappa = \kappa_o = \gamma_o/(V_1V_2)^{\frac{1}{2}} \quad , \tag{27}$$

and the number of amplitude e-foldings in a length L is

$$N \simeq \gamma_o L/(V_1 c)^{\frac{1}{2}} \quad . \tag{28}$$

It remains to evaluate L for an inhomogeneous plasma. Following the previous discussion, we compute L from the equation

$$\int_o^L [k_o - k_2 - k_1(x)] \, dx = \pm \frac{1}{2} \quad , \tag{29}$$

where $\omega_1^2 = \omega_p^2(x) + 3v_e^2k_1^2(x)$. For a linear profile $\omega_p^2(x) = \omega_{po}^2(1 \pm x/L_n)$,

we obtain

$$L^2 = 12\, k_o L_n\, \lambda_D^2 . \qquad \text{(linear)} \tag{30}$$

For a parabolic profile $\omega_p^2(x) = \omega_{po}^2(1 \pm x^2/L_n^2)$, we obtain

$$L^3 = 18\, k_o L_n^2\, \lambda_D^2 , \qquad \text{(parabolic)} \tag{31}$$

where λ_D is the Debye length. Use of Eqs. (30) and (10) in Eq. (28) leads to the usual convective threshold for a linear density profile

$$\frac{v_o^2}{c^2} = \frac{2}{k_o L_n} , \tag{32}$$

valid for N = 1.

III. SRS EXPERIMENTS COMPARED

Stimulated Raman scattering has been observed in three general types of experiments: 1) high intensity irradiation of solid targets, 2) solid or foam target experiments specifically designed to measure SRS, and 3) scattering from large underdense plasmas prepared by ionizing a gas. Examples of Type (1) are the Livermore experiment by Phillion et al.[10] on Shiva and by Drake et al.[11] on Novette, and the Rochester experiments reported by Tanaka et al.[12] and Seka et al.[13] In these experiments the local scalelength and temperature in the interaction region could not be measured. The density profile is linear or exponential with L_n calculated from hydrocodes to be of order 50 μm. The value of T_e is usually time and space averaged over the corona. Examples of Type (2) experiments are the one at NRC Ottawa reported by Walsh et al.[14], the UCLA-Rochester-Yale collaboration reported by Figueroa et al.[15] and the KMSF work by Shepard et al.[16] In Ref.

14, the plasma was made by 1.06-μm laser light on a solid target, and the scattering was done at 10.6-μm after a delay. In Ref. 15, the plasma was made by 1.06-μm light on a thin foil, whose thickness controlled the maximum density, and the scattering was done at 0.35 μm. In both cases it was possible to operate at the density maximum to gain the uniformity of a parabolic profile, and L_n could be measured independently. In Ref. 16, 0.53 μm light on a gold foil was used, and L_n of a linear profile was measured by interferometry. Examples of Type (3) experiments are the CO_2 experiments at the University of Alberta, reported by Offenberger et al.[17]; at the University of Washington, reported by Watt et al.[18]; and the Amini experiment at UCLA, described in Part (I)[19]. At Alberta, the plasma was made from a neutral gas by the laser beam itself and was confined by a large magnetic field. This method did not allow control of the density gradient and temperature conditions, and indeed SRS was seen only during after-pulses when the conditions were favorable. In the Washington and UCLA experiments, the plasma was made by an underdense theta pinch with no possibility of steep ionization fronts containing densities above $n_c/4$. In all three cases, the density scalelengths were very long and could be measured by interferometry. However, though the background temperature could be measured, it was still not possible to determine the local, instantaneous T_e at the laser focus.

Typical parameters of these experiments are listed in Table I; a question mark follows those numbers that could not be measured but had to be guessed. Where a range of conditions was covered, a single representative case was chosen for the purposes of these calculations.

From the data given in Table I, we compute for each case the homogeneous threshold I_h from Eqs. (21) and (11), and the absolute threshold I_a from Eqs. (24) and (11). These are compared with the observed threshold intensities I_{obs} in Table II. The convective thresholds I_c for 1, 3, 5 and 10 e-foldings above noise are also given, as calculated using Eq. (26) for the strongly damped case (D) or Eq. (28) for the collisionless case (C). The interaction length L is found from Eq. (30) or (31), depending on the density profile. If Eq. (26) is used, I_c should be $<I_a$; if Eq. (28) is used, I_c should be $\gg I_a$. Only in example IIC is the choice ambiguous.

In calculating the damping, we have taken

$$\gamma_1 = \frac{1}{2}\nu_{ei} + \gamma_{LD} , \qquad \gamma_2 = \frac{1}{2}(n/n_c)\nu_{ei} , \tag{33}$$

where the electron-ion collision frequency is the high-frequency value given by Johnston and Dawson[20]:

$$\nu_{ei} = 2.9 \times 10^{-6}\, Zn\, \ell n\Lambda / T_{eV}^{3/2} \tag{34}$$

and[21]

$$\begin{aligned} \ell n\Lambda &= 23 - \ell n(Z\, n^{1/2}/T_{eV}^{3/2}) \qquad (T_{eV} < 10\, Z^2) \\ &= 24 - \ell n(n^{1/2}/T_{eV}) \qquad (T_{eV} > 10\, Z^2) . \end{aligned} \tag{35}$$

For high-Z targets a conjectured value of the effective Z was used, but our conclusions are not changed by the choice of Z. For the Landau damping rate, we used the asymptotic formula

$$\gamma_{LD} = \pi^{1/2}\, \omega_1\, \zeta^3\, e^{-\zeta^2} \tag{36}$$

where

$$\omega_1^2 = \omega_p^2 + 3k_1^2 v_e^2 \qquad (37)$$

and

$$\zeta^2 = \omega_1^2 / 2k_1^2 v_e^2 \ . \qquad (38)$$

Eq. (36) underestimates the damping for small ζ, so that the calculated thresholds are conservative.

Examining Table II, we see that all solid-target experiments of Type I show the existence of SRS at intensities well below I_c, which is the appropriate theoretical threshold if the plasma is finite or inhomogeneous, even if only one e-folding is assumed. The disagreement is too large to be explained by self-focusing or uncertainties in L_n. This fact has inspired theorists[22,23] to consider the effects of initial density fluctuations of various types, noise sources such as Thomson scattering or electron streams, or reflection from the critical layer. Unfortunately, the plasma conditions in these experiments are too uncertain for detailed comparisons with theory. Note that the strong-damping approximation is appropriate for the collisionless cases (IA) and (IB) because of the Landau damping associated with the high electron temperature. The values of I_a and I_c, however, are sensitive to the exact electron velocity distribution $f_e(v)$, which cannot be measured accurately. Even if $f_e(v)$ could be measured well, it may be the <u>result</u> of the instability rather than the initial condition.

The situation is considerably better with Type II experiments specifically designed for the study of SRS. In the Ottawa experiment, in which the density profile could be changed, no SRS was observed with the linear profile up to $I_o = 2 \times 10^{14}$ W/cm^2, in agreement with theory. With the parabolic profile, the measured threshold agrees with I_c for N = 3; thus, there would be no discrepancy if the initial noise level were only six intensity e-foldings below the detection threshold. In the KMS experiment, the threshold

is lower than expected by at least two orders of magnitude; indeed, case (IIB) has the target conditions of a Type I experiment and differs only in that L_n was independently measured. In the Rochester-UCLA experiment, both Eq. (26) and Eq. (28) gave values of I_c near I_a, and neither approximation was valid for all values of N. It is clear, however, that I_{obs} is at least one order of magnitude below the calculated value.

Type III experiments in gas targets are amendable to more detailed measurements of the plasma conditions, particularly of the scalelength L_n. In the Alberta experiment the observed threshold is in good agreement with the absolute threshold, and it does not seem necessary to assume laser heating to T_e = 100 eV to explain the results. By contrast, the first report of SRS, by the University of Washington group[18], has a threshold at least three orders of magnitude below I_c and almost as low as I_h. In the UCLA work reported in the companion paper[19], the observed threshold agrees with I_c for $N \simeq 2$. However, the initial noise level was shown to be inconsistent with such a small number of e-foldings.

In conclusion, no experiment has shown a threshold higher than expected, and only cases IIA, IIIA, and IIIC in Table II have $I_{obs} \simeq I_a$ or I_c. The initial fluctuation level was not measured in cases IIA and IIIA, so that it is not possible to say whether the agreement was fortuitous or real.

IV. RAMAN EXCITATION OF SPATIALLY DAMPED PLASMA WAVES

The substantial discrepancy between theory and experiment evident in Table II can be removed by a minor modification of the theory. Instead of neglecting the plasma waves' group velocity V_1 in Eq. (12), we retain it. Equation (19) and the identical equation for E_2 now have solutions of the form $A\exp(\kappa_+ x) + B\exp(\kappa_- x)$, where $\kappa_\pm$ are the roots given by Eq. (22). It

will be convenient to define

$$\alpha \equiv \frac{1}{2}(\kappa_1 - \kappa_2) , \qquad \beta \equiv (\kappa_a^2 - \kappa_o^2)^{\frac{1}{2}} , \tag{39}$$

where κ_a and κ_o are, as before, $\kappa_a = (\kappa_1 + \kappa_2)/2$ and $\kappa_o = \gamma_o(V_1V_2)^{\frac{1}{2}}$. Equation (22) can then be written

$$\kappa_\pm = \alpha \pm \beta , \tag{40}$$

with β real as long as $\kappa_o < \kappa_a$. The daughter waves now have the form

$$n_1(x) = Ae^{\kappa_+ x} + Be^{\kappa_- x} \tag{41}$$

$$E_2(x) = Ce^{\kappa_+ x} + De^{\kappa_- x} . \tag{42}$$

The behavior of these roots is shown in Fig. 1. For each value of $\kappa_o < \kappa_a$ there are two possible values of κ, given by Eq. (40). These merge at the top of the parabola, where $\kappa_o = \kappa_a$. For $\kappa_o > \kappa_a$, no steady-state, spatially exponential solutions are possible, but for $\kappa_o >> \kappa_a$ the collisionless approximation of Eq. (27) is valid and is shown schematically as $I_c(C)$. When $I_o = 0$, $n_1(x)$ and $E_2(x)$ are uncoupled, and Eqs. (39) and (40) give $\kappa_+ = \kappa_1$, $\kappa_- = -\kappa_2$. In this case, κ_+ obviously represents the plasma wave, which is damped as it convects to the left, and κ_- the reflected wave, which is damped at its own rate as it convects to the right. When $I_o > 0$, both n_1 and E_2 are mixtures of the κ_+ and κ_- exponentials, both of which increase to the right when κ_o exceeds the homogeneous threshold κ_h, as can be seen from Eq. (20). The strong-damping approximation, Eq. (25), corresponds to the left branch of Fig. 1, shown as the thick line labeled $I_c(D)$, and is tantamount to setting $A = C = 0$ in Eqs. (41) and (42). Retaining the $\exp(\kappa_+ x)$ terms drastically

changes the nature of the solution.

Since both κ_+ and κ_- are >0 for $\kappa_o < \kappa_a$, let both $n_1(x)$ and $E_2(x)$ start from the noise levels $n_1^o \equiv n_1(0)$ and $E_2^o \equiv E_2(0)$ at the boundary x = 0. That this choice is the most reasonable one is not obvious; it will be discussed fully in Sec. VI. Substituting Eqs. (41) and (42) into Eqs. (17) and (18) gives

$$[A(\kappa_1 - \kappa_+) - \bar{a}_1 C]\, e^{\kappa_+ x} + [B(\kappa_1 - \kappa_-) - \bar{a}_1 D]\, e^{\kappa_- x} = 0 \qquad (43)$$

$$[C(\kappa_2 + \kappa_+) - \bar{a}_2 A]\, e^{\kappa_+ x} + [D(\kappa_2 + \kappa_-) - \bar{a}_2 B]\, e^{\kappa_- x} = 0 \,. \qquad (44)$$

Each square bracket must be zero for these equations to hold at all x. Using the identities $\kappa_1 - \kappa_- = \kappa_2 + \kappa_+ = \kappa_a + \beta$, $\kappa_1 - \kappa_+ = \kappa_2 + \kappa_- = \kappa_a - \beta$, $\bar{a}_1\bar{a}_2 = \kappa_o^2 = \kappa_a^2 - \beta^2$, we find that only two independent relations can be obtained for A, B, C, and D. Thus, there are two undetermined coefficients, which we choose to be

$$n_1^o = A + B \,, \qquad E_2^o = C + D \,. \qquad (45)$$

Eqs. (43), (44), (40), and (45) then yield

$$2\beta n_1(x) = [(\beta + \kappa_a)n_1^o - \bar{a}_1 E_2^o]\, e^{(\alpha+\beta)x} + [(\beta - \kappa_a)n_1^o + \bar{a}_1 E_2^o]\, e^{(\alpha-\beta)x} \qquad (46)$$

$$2\beta E_2(x) = [(\beta - \kappa_a)E_2^o + \bar{a}_2 n_1^o]\, e^{(\alpha+\beta)x} + [(\beta + \kappa_a)E_2^o - \bar{a}_2 n_1^o]\, e^{(\alpha-\beta)x} \,. \qquad (47)$$

In the limit $\kappa_o = 0$, we have $\beta = \kappa_a$, $\alpha+\beta = \kappa_1$, and $\alpha-\beta = -\kappa_2$; and these reduce to $n_1 = n_1^o \exp(\kappa_1 x)$, $E_2 = E_2^o \exp(-\kappa_2 x)$, which are uncoupled, damped waves as expected. When $\kappa_o \neq 0$, the growth of each wave depends on the initial level not only of itself, but also of the other wave.

The noise amplitude n_1^o is either thermal or larger than thermal because of turbulence generated in the plasma production process. In either case it can be measured and interpreted as in Part (I). The amplitude E_2^o, however, can arise from at least three sources: 1) bremsstrahlung emission, 2) Thomson scattering from thermal fluctuations, or 3) scattering from an enhanced fluctuation level. As an example we consider the conditions of the experiment in Part (I). Bremsstrahlung is independent of I_o and can be calculated from the Planck radiation law for a black body. For T_e = 20 eV, $\lambda \simeq 10$ μm, and spot diameter d = 300 μm, we obtain an emission of 8×10^{-3} W over a 2% wavelength range around 10 μm. Since the plasma is optically thin, this figure should be reduced by the ratio of absorption length to plasma length, or >100, as found in the heating calculation of (I). Thus the bremsstrahlung noise source is $<10^{-4}$ W. The level of CO_2 Thomson scattering from noise was found in (I) to be $P_s \simeq 10^{-11} P_o$. This should be halved because only half the plasma length of 10 cm can contribute to the noise at x = 0. If $P_o = 10^8$ W, we have $P_s \simeq 5 \times 10^{-4}$ W, which is somewhat larger than the bremsstrahlung emission; but this varies with P_o. If the plasma is slightly turbulent, with an oscillation level n_1/n_o and correlation length L_c, the reflectivity from the fluctuations can be estimated from the Bragg scattering formula $R = (0.5\, r_o \lambda_o n_1 L_c)^2$, where r_o is the classical electron radius. This can be larger than P_s/P_o above, depending on the values of n_1 and L_c.

Since it is not possible to determine E_2^o with any degree of certainty, we propose the following procedure for prescribing E_2^o for given n_1^o. At the homogenous threshold $\kappa_o^2 = \kappa_h^2 = \kappa_1 \kappa_2$, the pump intensity is just sufficient to sustain a constant level of waves against their damping mechanisms and is insufficient to excite these waves above their initial level. Under these conditions, the finite interaction region should blend in with the rest of the plasma, and there should be no gradients anywhere. Hence, we evaluate Eqs. (46)

and (47) for $\kappa_o = \kappa_h$, whereupon $\alpha = \beta$, $\beta - \kappa_a = -\kappa_2$, and $\beta + \kappa_a = \kappa_1$:

$$2\alpha n_1(x) = (\kappa_1 n_1^o - \bar{a}_1 E_2^o) e^{2\alpha x} + (\bar{a}_1 E_2^o - \kappa_2 n_1^o) \qquad (48)$$

$$2\alpha E_2(x) = (\bar{a}_2 n_1^o - \kappa_2 E_2^o) e^{2\alpha x} + (\kappa_1 E_2^o - \bar{a}_2 n_1^o) \quad . \qquad (49)$$

For these to be independent of x, the coefficients of $e^{2\alpha x}$ must vanish; thus

$$E_2^o/n_1^o = \kappa_1/\bar{a}_{1h} = a_{2h}/\kappa_2 \quad , \qquad (50)$$

where $\bar{a}_{1h}$ and $\bar{a}_{2h}$ are to be evaluated at $\kappa_o = \kappa_h$. As a check, we may substitute Eq. (50) into Eqs. (48) and (49) to obtain

$$2\alpha n_1(x) = (\kappa_1 - \kappa_2)\, n_1^o \qquad (51)$$

$$2\alpha E_2(x) = (\kappa_1 - \kappa_2)\, E_2^o \qquad (52)$$

The definition of α, Eq. (39), then gives $n_1(x) = n_1^o$, $E_2(x) = E_2^o$. To evaluate $\bar{a}_{1h}$ and $\bar{a}_{2h}$ in terms of $\bar{\alpha}_1$ and $\bar{\alpha}_2$, we note that $\bar{a}_1$ and $\bar{a}_2$ are proportional to E_o, so that $\bar{a}_1 = (\kappa_o/\kappa_h)\bar{a}_{1h}$, $\bar{a}_2 = (\kappa_o/\kappa_h)\bar{a}_{2h}$, and the term $\bar{a}_1 E_2^o$ in Eq. (46) can be written $(\kappa_o/\kappa_h)\kappa_1 n_1^o$, using Eq. (50). Similarly, the term $\bar{a}_2 n_1^o$ in Eq. (47) becomes $(\kappa_o/\kappa_h)\kappa_2 E_2^o$. Finally, κ_1/κ_h and κ_2/κ_h can be written in terms of the small quantity

$$\varepsilon \equiv (\kappa_2/\kappa_1)^{\frac{1}{2}} \qquad (53)$$

to give

$$2\beta n_1(x) = n_1^o[(\beta + \kappa_a - \kappa_o/\varepsilon) e^{(\alpha+\beta)x} + (\beta - \kappa_a + \kappa_o/\varepsilon) e^{(\alpha-\beta)x}] \qquad (54)$$

$$2\beta E_2(x) = E_2^o[(\beta - \kappa_a + \varepsilon\kappa_o) e^{(\alpha+\beta)x} + (\beta + \kappa_a - \varepsilon\kappa_o) e^{(\alpha-\beta)x}] \quad . \qquad (55)$$

These equations describe separately the spatial growth of n_1 and E_2 under

the prescription that n_1^o and E_2^o are related by the condition of homogeneity at $\kappa_o = \kappa_h$. The solution for $\kappa_o < \kappa_h$ cannot be trusted, but we shall see that for $\kappa_o >> \kappa_h$ the solution is insensitive to the exact prescription that we have chosen.

The inaccuracy of the finite interaction length model for $\kappa_o < \kappa_h$ is illustrated in Fig. 2. When $\kappa_o = 0$, initial levels n_1^o and E_2^o are assumed to exist outside the region $0 < x < L$, but these levels are zero inside the region. Fig. 2A represents the case where the plasma wave convection velocity V_1 is neglected ab initio; both n_o and E_2 then decay from the left at the rate given by Eq. (25): $\kappa = -\kappa_1\kappa_2/(\kappa_1 - \kappa_2)$. Fig. 2B schematically shows the present case, where V_1 is kept; E_2 then decays with $\kappa = -\kappa_2$ as it propagates from the left, and n_1 decays with $\kappa = \kappa_1$ as it propagates from the right. In both pictures, $n_1(x)$ and $E_2(x)$ become flat across the region by the time I_o has been increased to the homogeneous threshold. However, in case (A) n_1^o and E_2^o are arbitrary, while in (B) they are related by Eq. (50). In practice, thermal or hyperthermal noise generation occurs within the region as well as outside it, and a small pump intensity $0 < I_o < I_h$ is not necessary to overcome the damping. In fact, the instability can start at many places at once, and the interference of these waves depends on the initial hot spots. Once a dominant mode takes hold, however, the growth for $I_o >> I_h$ does not depend on exactly how it emerged from the noise; all theories are limited to this regime anyway.

Equations (54) and (55) lead to quite a different picture for the wave amplitude profiles from the usual one given by Eq. (26). Both $n_1(x)$ and $E_2(x)$ grow at the fast spatial rate $e^{(\alpha+\beta)x}$ instead of the slow rate $e^{(\alpha-\beta)x}$ corresponding to Eq. (26). Secondly, $n_1(x)$ and $E_2(x)$ grow at different rates, with n_1 e-folding more times than E_2 in a given length L. To see this, consider the growth at the limit of validity of Eqs. (54) and (55); namely, at $\kappa_o = \kappa_a$, the absolute threshold. We then have $\beta = 0$, and the

exponentials $e^{\pm\beta x}$ can be expanded to obtain the values

$$n_1(x) = n_1^o\, e^{\alpha x}[1 + \kappa_a x(1 - \varepsilon^{-1})] \tag{56}$$

$$E_2(x) = E_2^o\, e^{\alpha x}[1 - \kappa_a x(1 - \varepsilon)] \quad . \tag{57}$$

Thus, $(n_1/n_1^o)^2$ is generally larger than $(E_2/E_2^o)^2$ because of the factor ε^{-1}.

The behavior of the solution of Eqs. (54) and (55) is illustrated in Figs. 3-5 for the conditions of the experiment of Part (I), where the scale-length L_n = 15 cm gives a turning-point distance L = 0.15 cm. In Fig. 3, the normalized amplitudes n_1/n_1^o and E_2/E_2^o, starting at 1 at x=0, are shown vs. x for various intensities I_o between 0 and I_a. Both n_1/n_1^o and E_2/E_2^o are >1 for $I_o < I_h$ and eventually reach an exponentiation rate dominated by the $e^{(\alpha+\beta)x}$ term. At $I_o = I_h$, there is a concellation within the parentheses multiplying the exponential factors, and both n_1/n_1^o and E_2/E_2^o are unity everywhere. This cancellation is extremely sharp for n_1. When $I_o > I_h$, both amplitudes decrease to 0 and then become negative, indicating a phase change relative to the noise fluctuation; this occurs very close to x = 0 for the plasma wave. The phase change has no physical significance, being a consequence of the adhoc condition relating n_1^o to E_2^o; and the results are not expected to be accurate in the neighborhood of this phase change. When $I_o >> I_h$, both $n_1(x)$ and $E_2(x)$ grow at essentially the rate $e^{(\alpha+\beta)x} \simeq e^{\kappa 1 x}$. Thus the exponentiation length is scaled to the plasma wave damping length, which is generally much shorter than the growth length of Eq. (26), which corresponds to the $e^{(\alpha-\beta)x}$ term. Note that the value of L in the experiment, corresponding to L_n (parabolic) = 15 cm, is ≃0.15 cm. It is clear from Fig. 3 that $n_1(x)$ should have saturated by x = 0.15 cm at $I_o = 10^{11}$ W/cm^2; we treat the saturation in Sec. V.

Figure 4 shows the intensity e-folding of $n_1(L)$ and $E_2(L)$ at L = 0.07 cm as I_o is increased. Note that the plasma wave e-folds ≈15 times more than the reflected wave, and that the number of e-foldings is sufficent to reach saturation even when I_o is much less than I_a. The behavior near I_h, as previously explained, has no particular significance. Note also that the largest growth occurs for I_o somewhat less than I_a. Fig. 5 shows more graphically the wave shapes at $I_o = 10^{11}$ W/cm^2. After the initial phase reversal, both $n_1(x)$ and $E_2(x)$ grow with an exponentiation length $\simeq 1/(\alpha+\beta) \simeq 1/\kappa_1 = 4.4 \times 10^{-3}$ cm. By comparison, the old solution of Eq. (26) has an exponentiation length 25 times longer. The damping length of the light wave E_2 is 238 cm.

In the limit $V_1 \to 0$, one might expect the solution of Eq. (54) and (55) to reduce to that of Eq. (26), but it does not. To show this, we rewrite Eqs. (54) and (55) in terms of quantities which remain finite as $\varepsilon^2 \equiv \gamma_2 V_1/\gamma_1 V_2 \to 0$:

$$\frac{n_1}{n_1^o} = \frac{1}{2}\left[1 - \frac{g_o f/\varepsilon - 1}{(1 - g_o^2 f^2)^{1/2}}\right] e^{\kappa_+ x} + \frac{1}{2}\left[1 + \frac{g_o f/\varepsilon - 1}{(1 - g_o^2 f^2)^{1/2}}\right] e^{\kappa_- x} \qquad (58)$$

$$\frac{E_2}{E_2^o} = \frac{1}{2}\left[1 - \frac{1 - \varepsilon g_o f}{(1 - g_o^2 f^2)^{1/2}}\right] e^{\kappa_+ x} + \frac{1}{2}\left[1 + \frac{1 - \varepsilon g_o f}{(1 - g_o^2 f^2)^{1/2}}\right] e^{\kappa_- x} \quad , \qquad (59)$$

where

$$f(\varepsilon) \equiv 2\varepsilon/(1 + \varepsilon^2) \qquad (60)$$

$$g_o \equiv \gamma_o/\gamma_h = \gamma_o/(\gamma_1\gamma_2)^{1/2} \qquad (61)$$

$$\kappa_\pm = \alpha \pm \beta = (\kappa_2/\varepsilon f)\left[1 \pm (1 - g_o^2 f^2)^{1/2}\right] - \kappa_2 \; . \qquad (62)$$

The square root is proportional to β and is positive for $I_o < I_a$. As $\varepsilon \to 0$, $f(\varepsilon) = 2\varepsilon + 0(\varepsilon^2)$ and we have

$$\frac{n_1}{n_1^o} \to (1 - g_o)\, e^{\kappa_+ x} + g_o e^{\kappa_- x} \tag{63}$$

$$\frac{E_2}{E_2^o} \to g_o(1 - g_o)\varepsilon^2\, e^{\kappa_+ x} + e^{\kappa_- x} \tag{64}$$

$$\kappa_+ \to \kappa_2/\varepsilon^2 - \kappa_2 = \kappa_1 - \kappa_2 \simeq \kappa_2/\varepsilon^2 \tag{65}$$

$$\kappa_- \to \kappa_2(g_o^2 - 1) = (\gamma_o^2 - \gamma_h^2)/\gamma_1 V_2 \,. \tag{66}$$

We see that $n_1 = n_1^o$ and $E_2 = E_2^o$ at the homogeneous threshold $g_o = 1$, as required; and that, for $g_o > 1$, n_1/n_1^o grows as $\simeq \exp(\kappa_1 x)$. Applying L'Hospital's rule, we see that E_2/E_2^o is also dominated by the $\exp(\kappa_1 x)$ terms as $\varepsilon \to 0$ and does not converge to the usual solution $\exp(\kappa_- x)$. Only a change in boundary condition will give this, as will be seen later.

Figure 6 shows the spatial behavior of $(n_1/n_1^o)^2$ and $(E_2/E_2^o)^2$ for fixed κ_2 and g_o and various values of ε. The horizontal axis is scaled to the n_1 damping length. As seen from Eq.-(63), n_1 is not sensitive to the value of ε, but E_2 is. The main effect of ε on E_2 is to move the phase-reversal point to larger x as ε is decreased. Both n_1 and E_2 eventually grow as $\exp(\kappa_1 x)$, and therefore rise steeply as $V_1 \to 0$.

This is our primary result, and it can explain the observations of SRS well below the absolute threshold in short scalelength plasmas. This conclusion is not sensitive to the choice of prescription for E_2^o/n_1^o.

V. EFFECTS OF SATURATION ON REFLECTIVITY

Because of the rapid spatial growth of $n_1(x)$, the plasma wave is

likely to saturate within the region of relative homogeneity. In our previous studies of stimulated Brillouin scattering[24], we found that the most likely saturation mechanism was the nonlinear frequency shift, which causes the electrostatic wave to get out of phase with the ponderomotive drive. The waves then propagate without growing, forming a plateau in the amplitude profile. The reflectivity then increases slowly with the length of this plateau. The same mechanism can be operative in Raman scattering, but no detailed space-time measurements of the amplitude profile have yet been made. Analysis of the nonlinear behavior is outside the scope of this paper, but we can calculate the absolute value of the SRS reflectivity assuming different saturation levels n_1/n_o. Figure 7 gives an example of such a calculation applying Eqs. (54) and (55) to parameters pertinent to Part I. The reflectivity R is defined as $R = E_2^2(x)/E_o^2$, where x is determined by the condition that $n_1(x)/n_o$ be at the given saturation value. In all cases the value of x was between 0.03 and 0.05 cm, well within the interaction length L of 0.15 cm calculated for a parabolic profile with $L_n = 15$ cm. The value of R depends on the noise level n_1^o/n_o assumed; we have taken the rough value 3.6×10^{-7} estimated in Part I. Figure 7 shows that the observed vlaues of R in the range 10^{-4}-10^{-3} correspond to saturation levels of order 20±10%. The slope of the curves in the range $I_o = (1\text{-}3) \times 10^{11}$ W/cm^2 is smaller than observed, but we have not accounted for Bragg reflection from the plateau region of the wave profile. This effect can also lower the saturation level n_1/n_o required to give the observed value of R.

VI. EFFECT OF BOUNDARY CONDITIONS

In Eq. (45) we chose to express the unknown coefficients A, B, C, and D in terms of the noise levels n_1^o and E_2^o at x = 0. This seems reasonable, since both the exponential factors $\exp(\kappa_+ x)$ and $\exp(\kappa_- x)$ increase to the

right. However, it can be argued that the plasma wave n_1 should start from noise at x = L, since its group velocity is to the left, and that therefore the appropriate noise levels are E_2^o and $n_1^L = n_1(L)$. To investigate this we replace Eq. (45) with

$$n_1^L = Ae^{\kappa_+ L} + Be^{\kappa_- L}, \qquad E_2^o = C + D \tag{67}$$

and eliminate A, B, C and D as before, obtaining

$$\begin{aligned} n_1(x) = \Delta^{-1}\{&[(\beta + \kappa_a)e^{-\kappa_+ L} n_1^L - \bar{a}_1 e^{-2\beta L} E_2^o]\, e^{\kappa_+ x} \\ &+ [(\beta - \kappa_a)e^{-\kappa_+ L} n_1^L + \bar{a}_1 E_2^o]\, e^{\kappa_- x}\} \end{aligned} \tag{68}$$

$$\begin{aligned} E_2(x) = \Delta^{-1}\{&[(\beta - \kappa_a)e^{-2\beta L} E_2^o + \bar{a}_2 e^{-\kappa_+ L} n_1^L]\, e^{\kappa_+ x} \\ &+ [(\beta + \kappa_a)E_2^o - \bar{a}_2 e^{-\kappa_+ L} n_1^L]\, e^{\kappa_- x}\} \end{aligned} \tag{69}$$

where

$$\Delta = \beta + \kappa_a + (\beta - \kappa_a)e^{-2\beta L} \tag{70}$$

To relate the values of n_1^L and E_2^o, we can again use the device of specifying that $n_1(x)$ and $E_2(x)$ be uniform at the homogeneous threshold $\kappa_o = \kappa_h$. We find that the previous relations

$$\bar{a}_1 E_2^o = (\kappa_o/\varepsilon) n_1^L, \qquad \bar{a}_2 n_1^L = \kappa_o \varepsilon E_2^o \tag{71}$$

used in Eqs. (54) and (55) still obtain. Eqs. (68) and (69) then become

$$\frac{n_1(x)}{n_1^L} = \Delta^{-1}\{[(\beta + \kappa_a)e^{-\kappa_+ L} - (\kappa_o/\varepsilon)e^{-2\beta L}]\ e^{\kappa_+ x} + [(\beta - \kappa_a)e^{-\kappa_+ L} + \kappa_o/\varepsilon]\ e^{\kappa_- x}\} \tag{72}$$

$$\frac{E_2(x)}{E_2^o} = \Delta^{-1}\{[\varepsilon\kappa_o e^{-\kappa_+ L} + (\beta - \kappa_a)e^{-2\beta L}]\ e^{\kappa_+ x} + [-\varepsilon\kappa_o e^{-\kappa_+ L} + \beta + \kappa_a]\ e^{\kappa_- x}\} \tag{73}$$

The reflection amplitude is

$$\frac{E_2(L)}{E_2^o} = \Delta^{-1}[2\beta e^{\kappa_- L} + \varepsilon\kappa_o(1 - e^{-2\beta L})] \ . \tag{74}$$

Fig. 8 shows the behavior of Eqs. (72) and (73) for an intensity well below the absolute threshold. One sees that both n_1 and E_2 grow at the slower rate exp $(\kappa_- x)$, as previously believed. However, the boundary condition makes no physical sense as it stands. At the left boundary, n_1 is e^4 times noise at $x = \varepsilon$ and drops discontinuously to the noise level at $x = -\varepsilon$. Since waves are convecting to the left, it is unreasonable for n_1 to decay discontinuously going from right to left. [Note added in proof: The referee has suggested that a two-region model in which the pump vanishes for $-\delta < x < 0$ but undriven plasma waves are allowed to exist in that range can explain the level $n_1 = e^4 n_1^L$ at $x = 0$. However, such a model would show that n_1 falls to noise level within a few damping lengths $1/\kappa_+$. Thus, starting a $x = -4/\kappa_+$, the plasma wave would have grown to e^4 times noise level by x=0. This is essentially the behavior predicted by the one-region model with n_1 set equal to noise at $x = -4/\kappa_+$. The one-region model and the two-region model are equally inexact representations of the real situation, in which the pump

intensity fades gradually; and it is gratifying that both models predict instability occurring for $L > 1/\kappa_+$, rather than $L > 1/\kappa_-$.]

At the right boundary, we see that n_1 grows from n_1^L to its maximum value in the interval $.09 < x < .10$ cm. In the interval $.08 < x < .09$, E_2 has approximately the same value, but n_1 does not grow at all. Solutions of this type have been computed previously in another connection[25] and can be explained as follows. Upon entering the interaction region at $x = L$, plasma waves are rapidly driven up from noise by the large ponderomotive force due to $E_o E_2$. At $x \simeq 0.09$, n_1 has reached such a large level that its damping is equal to the excitation. This balance is maintained from $x \simeq 0.09$ down to $x = 0$, which is the reason n_1 and E_2 have the same spatial behavior. Thus, the scalelength $1/\kappa_-$ represents not the growth length of n_1 (which is $1/\kappa_+$) but the variation of its saturation value when saturation is due to the balance between damping and excitation. Since there are other saturation mechanisms that can be more restrictive--such as harmonic generation, wavebreaking, or electron trapping--we have chosen to set n_1 equal to noise level at some point on the left and simply study the effect of various assumed saturation values.

A second reason for rejecting the n_1^L boundary condition is that it leads to inconclusive results; namely, to a growth length that depends sensitively on the ratio of n_1^L to E_2^o. By contrast, the n_1^o boundary condition gives the same spatial growth rate regardless of whether n_1^o is negligibly small, E_2^o is negligibly small, or neither is negligible. Details of these calculations are given in Appendix B.

VII. DISCUSSION

We have followed a well worn path in the treatment of SRS. The governing equations, Eqs. (4) and (5), are the same as those used by the original workers on the subject[1,3,5-7,26-29] as well as in subsequent papers[4,8,9,18, 30-32]. However, in previous work on laser-plasma interactions, either the damping γ_1 or the group velocity V_1 of the plasma wave was neglected in order to simplify the problem sufficiently to treat such effects as pump depletion or nonlinear saturation. We find that even the linear theory, which governs the behavior near threshold, cannot be made to agree with experiment unless both damping and convection are included. This is particularly true of high-intensity experiments where KT_e is in the kilovolt range and both Landau damping and the plasma wave group velocity are appreciable.

When γ_1 and V_1 are both taken into account, and a reasonable boundary condition is used, SRS below the absolute threshold can occur over short distances on the scale of the damping length V_1/γ_1. The physical reason is apparently that any energy going into the plasma wave decays with this spatial scalelength as it propagates in the $\underline{k}_1$ direction, and therefore it is unnatural for the amplitude to be more constant in space than this. The reflected wave CO_2 has an almost infinite damping length in an underdense plasma, but since it

is excited by $n_1(x)$, it also must have a steep spatial profile. There is no a priori reason why the pump cannot deposit its energy in a thin layer of plasma once a localized plasma wave has been driven up from noise.

The behavior of the instability near the homogeneous threshold is not easily predictable. It is possible, for instance, for plasma waves to start simultaneously at two nearby points in space and for these waves to interfere constructively or destructively at later times. The initial noise conditions depend on the way the plasma was created; even when the plasma is nearly thermal, it is the small deviations from equilibrium that govern the initiation of the instability. To achieve a tangible result, we have given a particular prescription for the relation between n_1^o and E_2^o. This formula may or may not be realistic, but the initial noise problem has not been treated successfully by any author. Fortunately, the behavior of the instability well above the homogeneous threshold is not greatly affected by the initial or boundary conditions, as long as reasonable ones are used, as discussed in Sec. VI.

To explain the low SRS threshold observed in inhomogeneous plasmas, Simon and Short[23] have proposed an interesting mechanism related to fast electrons generated at the quarter-critical layer. However, this mechanism does not explain the anomalies observed in experiments without a quarter-critical layer. By designing an apparatus that cannot have densities as high as $n_c/4$ (Part I), we have been able to remove ambiguities caused by the possible existence of fast electrons. Indeed, recent experiments at Rochester[33] have shown that the so-called "Raman gap" fills in when the $n_c/4$ layer is removed,

indicating a negative correlation between the $n_c/4$ layer and SRS. Though this paper does not address the problem of the Raman gap, we note in conclusion that our results can also explain the absence of SRS in high-density regions of a blow-off plasma. Both Landau and collisional damping are weak in those regions, and the damping length $1/\kappa_1$ becomes comparable to L. Only in the very underdense regions is Landau damping strong enough to make $\kappa_1 L >> 1$, thus allowing the phenomena described in this paper to occur.

ACKNOWLEDGMENTS

We acknowledge a useful conversation with K. Mima of Osaka University. This work was supported by the National Science Foundation, Grant No. ECS 83-10972; by the Lawrence Livermore Laboratory, Work Order No. 3446905; and by the U.S.D.O.E., Contract DE-AS08-85DP40205.

APPENDIX A

Steady-State Solutions Above the Absolute Threshold

For completeness we have also investigated the nature of time-independent solutions of Eqs. (4) and (4) at intensities above I_a. In that case β, as defined by Eq. (39), becomes imaginary , and the functions $n_1(x)$

and $E_2(x)$ have the form $e^{\alpha x}$ (A sin $\bar{\beta}x$ + B cos $\bar{\beta}x$), where

$$\bar{\beta} \equiv (\kappa_o^2 - \kappa_a^2)^{\frac{1}{2}} \quad . \tag{75}$$

In terms of the boundary values n_1^o at x = 0 and n_1^L at x = L, Eq. (19) now has the solution

$$n_1(x) = e^{\alpha x} [n_1^o \cos \bar{\beta}x + (n_1^L e^{-\alpha L} - n_1^o \cos \bar{\beta}L)(\sin \bar{\beta}x/\sin \bar{\beta}L)] \quad . \tag{76}$$

A similar equation obtains for $E_2(x)$. It is clear from this that if $\bar{\beta}L \geq \pi$, one can choose an interaction region of length L' < L such that sin $\bar{\beta}L'$ = 0 and $n_1(x)$ is not well defined. Since $\bar{\beta}$ increases rapidly with κ_o, as contrasted with β, which changes slowly for $\kappa_o^2 << \kappa_a^2$, these convective solutions are valid only over a limited range of intensities $I_o > I_a$.

We first consider solutions which start from noise at x = 0 and increase with x. Thus we choose the two unspecified boundary values to be n_1^o and E_2^o. Eqs. (17) and (18) now give

$$n_1(x) = e^{\alpha x}[n_1^o \cos \bar{\beta}x + \bar{\beta}^{-1}(\kappa_a n_1^o - \bar{a}_1 E_2^o) \sin \bar{\beta}x] \tag{77}$$

$$E_2(x) = e^{\alpha x}[E_2^o \cos \bar{\beta}x + \bar{\beta}^{-1}(\bar{a}_2 n_1^o - \kappa_a E_2^o) \sin \bar{\beta}x] \quad , \tag{78}$$

valid for $\kappa_o > \kappa_a$. To match smoothly onto the $\kappa_o < \kappa_a$ solution of Eqs. (54) and (55), we find that n_1^o and E_2^o must again be related by Eq. (50), viz., $\bar{a}_1 E_2^o = (\kappa_o/\varepsilon) n_1^o$, $\bar{a}_2 n_1^o = \kappa_o \varepsilon E_2^o$, giving

$$n_1(x) = n_1^o\, e^{\alpha x}[\cos\, \bar{\beta}x + (\kappa_a - \kappa_o/\varepsilon)\, \sin\bar{\beta}x/\bar{\beta}] \qquad (79)$$

$$E_2(x) = E_2^o\, e^{\alpha x}[\cos\, \bar{\beta}x - (\kappa_a - \varepsilon\kappa_o)\, \sin\bar{\beta}x/\bar{\beta}] \quad . \qquad (80)$$

At the absolute threshold $\kappa_o = \kappa_a$, both β and $\bar{\beta}$ vanish, and both Eqs. (54-55) and (79-80) reduce to

$$n_1(x) = n_1^o\, e^{\alpha x}[1 - (\varepsilon^{-1} - 1)\kappa_a x] \qquad (81)$$

$$E_2(x) = E_2^o\, e^{\alpha x}[1 - (1 - \varepsilon)\kappa_a x] \quad . \qquad (82)$$

As κ_o increases well beyond κ_a, one might expect the damping of both waves to become negligible, so that each wave grows in the direction of its propagation, as shown in Fig. 9. In that case we must choose E_2^o and n_1^L to be the boundary values specified by the initial noise. Eqs. (17) and (18) are then satisfied by the functions

$$n_1(x) = \frac{1}{D}\,[(\bar{\beta}n_1^L e^{-\alpha L} + \bar{a}_1 E_2^o \sin\bar{\beta}L)\, e^{\alpha x}\cos\bar{\beta}x + (\kappa_a n_1^L e^{-\alpha L} - \bar{a}_1 E_2^o \cos\bar{\beta}L)\, e^{\alpha x}\sin\bar{\beta}x] \qquad (83)$$

$$E_2(x) = E_2^o e^{\alpha x}\cos\bar{\beta}x + \frac{1}{D}\,[\bar{a}_2 n_1^L e^{-\alpha L} + (\bar{\beta}\sin\bar{\beta}L - \kappa_a\cos\bar{\beta}L)E_2^o]\, e^{\alpha x}\sin\bar{\beta}x \qquad (84)$$

where

$$D \equiv \kappa_a \sin\bar{\beta}L + \bar{\beta}\cos\bar{\beta}L \quad . \qquad (85)$$

These obviously break down at intensities such that $D = 0$. If the noise sources n_1^L and E_2^o are related by Eq. (50), we have

$$n_1(x)/n_1^L = D^{-1}e^{\alpha x}[\bar{\beta}e^{-\alpha L} + \varepsilon^{-1}\kappa_o \sin\bar{\beta}L)\cos\bar{\beta}x + (\kappa_a e^{-\alpha L} - \varepsilon^{-1}\cos\bar{\beta}L)\sin\bar{\beta}x] \quad (86)$$

$$E_2(x)/E_2^o = e^{\alpha x}[\cos\bar{\beta}x + D^{-1}(\kappa_o \varepsilon e^{-\alpha L} + \bar{\beta}\sin\bar{\beta}L - \kappa_a \cos\bar{\beta}L)\sin\bar{\beta}x] \quad (87)$$

The total amplification is then

$$n_1(0)/n_1^L = D^{-1}(\bar{\beta}e^{-\alpha L} + \varepsilon^{-1}\kappa_o \sin\bar{\beta}L) \quad (88)$$

$$E_2(L)/E_2^o = D^{-1}(\bar{\beta}e^{\alpha L} + \kappa_o \varepsilon \sin\bar{\beta}L) \quad . \quad (89)$$

In the zero-damping limit, we have $\alpha = \kappa_a = 0$ and $\bar{\beta} = \kappa_o$; Eqs. (83) and (84) then reduce to

$$n_1(x)/n_1^L = \cos\kappa_o x/\cos\kappa_o L + \varepsilon^{-1}(\tan\kappa_o L \cos\kappa_o x - \sin\kappa_o x) \quad (90)$$

$$E_2(x)/E_2^o = \cos\kappa_o x + \tan\kappa_o L \sin\kappa_o x + \varepsilon\sin\kappa_o x/\cos\kappa_o L \quad . \quad (91)$$

The total amplification is

$$n_1(0)/n_1^L = \sec\kappa_o L + \varepsilon^{-1} \tan\kappa_o L \quad (92)$$

$$E_2(L)/E_2^o = \sec\kappa_o L + \varepsilon \tan\kappa_o L \quad , \quad (93)$$

these results again depending on Eq. (50). It is clear that these solutions fail and absolute instabilities must be considered when $\kappa_o L \simeq \pi/2$.

For completeness we have investigated the transition between large-damping solutions growing from the left and zero-damping solutions growing in

opposite directions, as in Fig. 9, when κ_o is increased beyond κ_a. Figure 10 shows the behavior of Eqs. (79) and (80) for κ_o^2 varying from κ_a^2 to $\simeq 2\kappa_a^2$. At $I_o \simeq 2.5 \times 10^{11}$ W/cm^2, $n_1(L)$ rapidly changes sign, passing through the value $n_1(L) = n_1^o$. Further increase in I_o, however, does not generate an n_1 profile resembling that in Fig. 9 even for $\bar{\beta}L > 2\pi$. Figure 11 is a plot of Eqs (86) and (87) and illustrates what happens when $n_1(x)$ is forced to be at the noise level n_1^L at $x = L$. The solution at $I_o = 1.64 \times 10^{11}$ W/cm^2, just above I_a, does not have the behavior shown in Fig. 9. As I_o passes through 2.3×10^{11} W/cm^2, D goes through zero and n_1 goes through infinity; the steady-state assumption is no longer valid. Figure 12 is a plot of Eqs. (90) and (91) with $\gamma_1 = \gamma_2 = 0$. Even with zero damping, the convective behavior depicted in Fig. 9 is never realized. This fact was of course known to those who have solved the time-dependent problem[7,8,9] but is not generally recognized.

APPENDIX B

Consequences of Reverse Boundary Condition

We give here further details on the solutions obtained when the plasma wave noise level is fixed at $x = L$ rather than at $x = 0$. When n_1^L and E_2^o are related by Eq. (71), which is the same as Eq. (50), the solution is given by Eqs. (72) and (73), and the behavior is shown in Fig. 8. When either noise source vanishes, the behavior is quite different.

If $E_2^o = 0$, the solution is

$$n_1(x) = n_1^L \, e^{-\kappa_+(L-x)} \, \frac{\kappa_a + \beta - (\kappa_a - \beta) \, e^{-2\beta x}}{\kappa_a + \beta - (\kappa_a - \beta) \, e^{-2\beta L}} \tag{94}$$

$$E_2(x) = \bar{a}_2 n_1^L \, e^{-\kappa_+(L-x)} (1 - e^{-2\beta x})/\Delta \, , \tag{95}$$

where Δ is the same denominator as in Eq. (94).

Using Eqs. (7) and (15) for $\bar{a}_2$, we can write $E_2(L)$ as

$$E_2(L) = n_1^L \, 6^{1/2} \, \pi e \kappa_o \lambda_D \, (1 - e^{-2\beta L})/\Delta. \qquad (96)$$

The spatial behavior of n_1 and E_2 is shown in Fig. 13a. It is seen that n_1 is below the noise level inside the interaction region, as is clear from Eq. (94).

If $n_1^L = 0$, the solution is

$$n_1(x) = \bar{a}_1 E_2^o \, e^{\kappa_- x}(1 - e^{-2\beta(L-x)})/\Delta \qquad (97)$$

$$E_2(x) = E_2^o \, e^{\kappa_- x}[\kappa_a + \beta - (\kappa_a - \beta)e^{-2\beta(L-x)}]/\Delta \, . \qquad (98)$$

The amplification of E_2 is

$$\frac{E_2(L)}{E_2^o} = e^{\kappa_- L} \, (2\beta/\Delta) \, . \qquad (99)$$

The spatial behavior is shown in Fig. 13b. In this case both waves grow at the slow rate exp $(\kappa_- x)$.

We now compare these results with those for n_1 being fixed at the noise level n_1^o at x=0, as assumed in the body of this paper. It is seen from Eqs. (46) and (47) that setting $n_1^o = 0$ or $E_2^o = 0$ does not change the spatial growth from the fast rate $\exp(\kappa_+ x)$. Fig. 14 shows the similarity of the spatial behavior of E_2 in these extreme cases.

We can also test the sensitivity of the scattered amplitude $E_2(L)$ to the assumed boundary conditions. For noise sources n_1^o and E_2^o, the

growth is exponential, so that Fig. 14 also shows $E_2(L)$ vs. L. For noise sources n_1^L and E_2^o, Eqs. (96) and (99) give $E_2(L)$ for $E_2^o = 0$ and $n_1^L = 0$, respectively. These are shown in Fig. 15. It is seen that $E_2(L)$ has an entirely different behavior depending on which noise source is dominant. We conclude that the n_1^L noise source does not give a physically reasonable result.

REFERENCES

1. M. N. Rosenbluth, Phys. Rev. Letters 29, 565 (1972).
2. F. F. Chen, in Laser Interaction and Related Plasma Phenomena, ed. by H. J. Schwarz and H. Hora, Vol. 3A, p. 291 (Plenum, New York, 1974).
3. D. Pesme, G. Laval, and R. Pellat, Phys. Rev. Letters 31, 203 (1973).
4. G. Picard and T. W. Johnston, Phys. Rev. Letters 51, 574 (1983).
5. D. W. Forslund, J. M. Kindel, and E. L. Lindman, Phys. Fluids 18, 1002 (1975).
6. C. S. Liu, N. N. Rosenbluth, and R. B. White, Phys. Fluids 17, 1211 (1974).
7. M. N. Rosenbluth, R. B. White, and C. S. Liu, Phys. Rev. Letters 31, 1190 (1973).
8. R. W. Harvey and G. Schmidt, Phys. Fluids 18, 1395 (1975).
9. A. Bers, D. J. Kaup, and A. H. Reiman, Phys. Rev. Letters 37, 182 (1976).
10. D. W. Phillion, D. L. Banner, E. M. Campbell, R. E. Turner, and K. G. Estabrook, Phys. Fluids 25, 1434 (1982).
11. R. P. Drake, R. E. Turner, B. F. Lasinski, K. G. Estabrook, E. M. Campbell, C. L. Wang, D. W. Phillion, E. A. Williams, and W. L. Kruer, Phys. Rev. Letters 53, 1739 (1984).
12. K. Tanaka, L. M. Goldman, W. Seka, M. C. Richardson, J. M. Soures, and E. A. Williams. Phys. Rev. Letters 48, 1179 (1982).
13. W. Seka, E. A. Williams, R. S. Craxton, L. M. Goldman, R. W. Short, and K. Tanaka, Phys. Fluids 27, 2181 (1984).
14. C. J. Walsh, D. M. Villeneuve, and H. A. Baldis, Phys. Rev. Letters 53, 1445 (1984).
15. H. Figueroa, C. Joshi, H. Azechi, N. A. Ebrahim, and K. Estabrook, Phys. Fluids 27, 1887 (1984).

16. C. L. Shepard, J. A. Tarvin, R. L. Berger, Gar. E. Busch, R. R. Johnson, and R. J. Schroeder, submitted to Phys. Fluids, 1985.

17. A. A. Offenberger, R. Fedosejevs, W. Tighe, and W. Rozmus, Phys. Rev. Letters 49, 371 (1982); Physica Scripta Topical Valume T2/2, 498 (1982).

18. R. G. Watt, R. D. Brooks, and Z. A. Peitrzyk, Phys. Rev. Letters 41, 170 (1978).

19. B. Amini and F. F. Chen, submitted to Phys. Fluids, 1985.

20. T. W. Johnston and J. M. Dawson, Phys. Fluids 16, 722 (1973).

21. D. L. Book, NRL Plasma Formulary (Naval Research Laboratory, Washington, DC, 1983).

22. K. Estabrook and W. L. Kruer, Phys. Rev. Letters 53, 465 (1984).

23. A. Simon and R. W. Short, Phys. Rev. Letters 53, 1912 (1984).

24. C. E. Clayton, C. Joshi, and F. F. Chen, Phys. Rev. Letters 51, 1656 (1983).

25. M. Porkolab and R. P. H. Chang, Phys. Fluids 13, 2054 (1970).

26. C. S. Liu, M. N. Rosenbluth, and R. B. White, Phys. Rev. Letters 31, 697 (1973).

27. R. White, P. Kaw, D. Pesme, M. N. Rosenbluth, G. Laval, R. Huff, and R. Varma, Nuclear Fusion 14, 45 (1974).

28. C. S. Liu, in Advances in Plasma Physics, ed. by A. Simon and W. B. Thompson, (Wiley, New York, 1976), Vol. 6, p. 121.

29. K. Mima and K. Nishikawa, in Basic Plasma Physics II, ed. by A. A. Galeev and R. N. Sudan (North-Holland, Amsterdam, 1984), Chap. 6.5.

30. V. Fuchs, Phys. Fluids 19, 1554 (1976) and 20, 1535 (1977).

31. F. Y. F. Chu and C. F. F. Karney, Phys. Fluids 20, 1728 (1977).

32. P. Koch and E. A. Williams, Phys. Fluids 27, 2346 (1984).

33. H. Figueroa and C. Joshi, in Laser Interaction and Related Plasma Phenomena, ed. by H. Hora and G. Miley (Plenum, New York, 1986), Vol. 7 (to be published).

TABLE CAPTIONS

I. Typical plasma conditions for nine experiments in which SRS was reported.

II. Calculated (I_h, I_a, I_c) and observed (I_{obs}) threshold intensities, in W/cm^2, for SRS in the experiments of Table I. (5E14 means 5×10^{14}). I_h and I_a are the homogeneous and absolute thresholds, respectively. I_c is the convective threshold calculated for various numbers N of e-foldings of amplitude above inital noise. D and C indicate whether the strong-damping (D) or collisionless (C) approximation was used for I_c.

TABLE I

	Experiment	λ_o(μm)	n(cm^{-3})	n/n_c	T_e(eV)	L_n	Profile
IA.	Shiva[10]	1.06	7×10^{19}	.07	5,000	100 μm (?)	linear
IB.	Novette[11]	0.53	3×10^{20}	.076	4,300(?)	170 μm (?)	linear
IC.	Rochester[12,13]	0.35	1×10^{21}	.11	1,000	50 μm (?)	linear
IIA.	Ottawa[14]	10.6	3×10^{17}	.03	100	300 μm 550 μm	linear parabolic
IIB.	KMS Fusion[16]	0.53	4×10^{19}	.01	2,000	80 μm	linear
IIC.	Rochester-UCLA[15]	0.35	7.7×10^{20}	.085	750	50 μm	parabolic
IIIA.	Alberta[17]	10.6	2.7×10^{17}	.02	45+	40 cm	parabolic
IIIB.	Washington[18]	10.6	2×10^{16}	.002	15	20 cm	parabolic
IIIC.	UCLA[19]	9.6	8×10^{16}	.066	19	15 cm	parabolic

TABLE II

	Experiment	Profile	I_{obs}	I_h	I_a	D/C	I_c N=1	I_c N=3	I_c N=5	I_c N=10
IA.	Shiva[10]	lin.	5E14	6.8E12	2.3E18	D	1.5E17	4.5E17	7.5E17	1.5E18
IB.	Novette[11]	lin.	1E14	8.9E13	7.5E18	D	3.2E17	9.6E17	1.6E18	3.2E18
IC.	Rochester[12,13]	lin.	4E14	7.2E12	1.2E16	C	2.3E16	2.0E17	5.7E17	2.3E18
IIA.	Ottawa[14]	lin.	>2E14	5.8E7	7.3E10	C	1.3E14	1.2E15	3.3E15	1.3E16
		para.	3E13	5.8E7	7.3E10	C	3.4E12	3.1E13	8.5E13	3.4E14
IIB.	KMS Fusion[16]	lin.	9E14	1.0E13	1.4E19	D	1.8E17	5.4E17	9.0E17	1.8E18
IIC.	Rochester-UCLA[15]	para.	<1E15	1.1E13	1.1E16	D	6.7E15	2.0E16	3.3E16	6.7E16
						C	1.1E15	9.6E15	2.7E16	1.1E17
IIIA.	Alberta[17]	para.	4E10	2.6E7	7.5E10	D	1.1E10	3.4E10	5.6E10	9.7E11
IIIB.	Washington[18]	para.	3E8	6.7E6	1.4E12	D	9.7E10	2.9E11	4.8E11	9.7E11
IIIC.	UCLA[19]	para.	1.3E11	5.2E7	7.4E11	D	7.7E10	2.3E10	3.8E11	7.7E11

FIGURE CAPTIONS

Fig. 1. The spatial damping rate κ, normalized to the plasma wave's spatial damping rate κ_1, as a function of pump intensity I_o, expressed as κ_o^2/κ_1^2, for $\kappa_2/\kappa_1 = 0.1$, an unrealistically large value chosen for emphasis. The labels I_h, I_a, and I_c refer to the threshold intensities of Table II. The collisionless convective threshold $I_c(C)$ is schematic only.

Fig. 2. Schematic of the wave amplitude behavior at $I_o = 0$ in the old (A) and new (B) models of SRS in a finite region.

Fig. 3. Spatial growth of plasma wave amplitude n_1/n_1^o (——) and reflected wave amplitude E_2/E_2^o (---) for various pump intensities I_o. Plasma parameters are: $n = 8 \times 10^{16}$ cm^{-3}, $T_e = 20$ eV, $\lambda_o = 9.58$ μm, $Z = 2$, homogeneous threshold $I_h = 4.57 \times 10^7$ W/cm^2, absolute threshold $I_a = 6.20 \times 10^{11}$ W/cm^2. The vertical scale changes from linear to logarithmic at ±1.

Fig. 4. Growth of plasma and reflected wave intensities with pump intensity I_o, for the conditions of Fig. 3 at $x = 0.07$ cm.

Fig. 5. Envelopes of the spatially varying amplitudes n_1/n_1^o and E_2/E_2^o for the conditions of Fig. 3, with $I_o = 10^{11}$ W/cm^2. The dashed lines form the envelope for both n_1/n_1^o and E_2/E_2^o for the $V_1 = 0$ result of Eq. (26), with an exponentiation length 0.11 cm. The dot-dash line (-·-) e-folds with a scalelength equal to V_1/γ_1. The vertical scale changes from linear to logarithmic at ±1.

Fig. 6. Wave intensities $(n_1/n_1^o)^2$ and $(E_2/E_2^o)^2$ as functions of $\kappa_1 x = \gamma_1 x/V_1$ for various values of $\varepsilon = (\kappa_2/\kappa_1)^{\frac{1}{2}}$. The values of $\kappa_2 = \gamma_2/V_2$ and $g_o = \gamma_o/\gamma_h$ are held fixed at $\kappa_2 = 2 \times 10^{-3}$, $g_o = 30$.

Fig. 7. Calculated SRS power reflectivity vs. I_o for various assumed saturation levels of the plasma wave. Plasma conditions are as in Fig. 3. A noise level of $n_1^o/n_o = 3.6 \times 10^{-7}$ was assumed.

Fig. 8. Spatial behavior of $n_1(x)$ and $E_2(x)$ when the noise levels are given as $n_1^L = n_1(L)$ and $E_2^o = E_2(0)$. The plasma conditions are: $n = 8 \times 10^{16}$ cm^{-3}, $T_e = 20$ eV, $Z = 2$ (He), $L = 0.1$ cm, $\lambda_o = 9.58$ μm, and $I_o = 2 \times 10^{11}$ W/cm^2 $\simeq I_a/3$.

Fig. 9. Classical picture of wave amplitude profiles in a convective instability.

Fig. 10. Steady-state spatial profiles of $n_1(x)$ and $E_2(x)$ for $I_o \geq I_a$. Plasma parameters are as in Fig. 3 except that $Z = 1$ and $I_a = 1.63 \times 10^{11}$ W/cm^2. The scale changes from linear to logarithmic at ±1.

Fig. 11. Same as Fig. 9, but with $n_1(x)$ starting from noise at $x = L = .07$ cm. Dashed lines are for $E_2(x)/E_2^o$.

Fig. 12. Same as Fig. 10, but with damping neglected.

Fig. 13. Spatial behavior of $n_1(x)$ and $E_2(x)$ when the boundary conditions are (a) $n_1(L) = n_1^L$, $E_2(0) = 0$; and (b) $n_1(L) = 0$, $E_2(0) = E_2^o$. Plasma conditions are as in Fig. 8.

Fig. 14. Spatial behavior of $E_2(x)$ or $E_2(L)$ when the boundary conditions are $n_1(0) = 0$, $E_2(0) = E_2^o$ (solid curve), and $n_1(0) = n_1^o$, $E_2(0) = E_2^o$ (dashed curve). Plasma conditions are as in Fig. 8.

Fig. 15. Dependence of scattered amplitude $E_2(L)$ on interaction length L when the boundary conditions are $n_1(L) = 0$, $E_2(0) = E_2^o$ (solid curve), and $n_1(L) = n_1^L$, $E_2(0) = 0$ (dashed curve). Plasma conditions are as in Fig. 8.

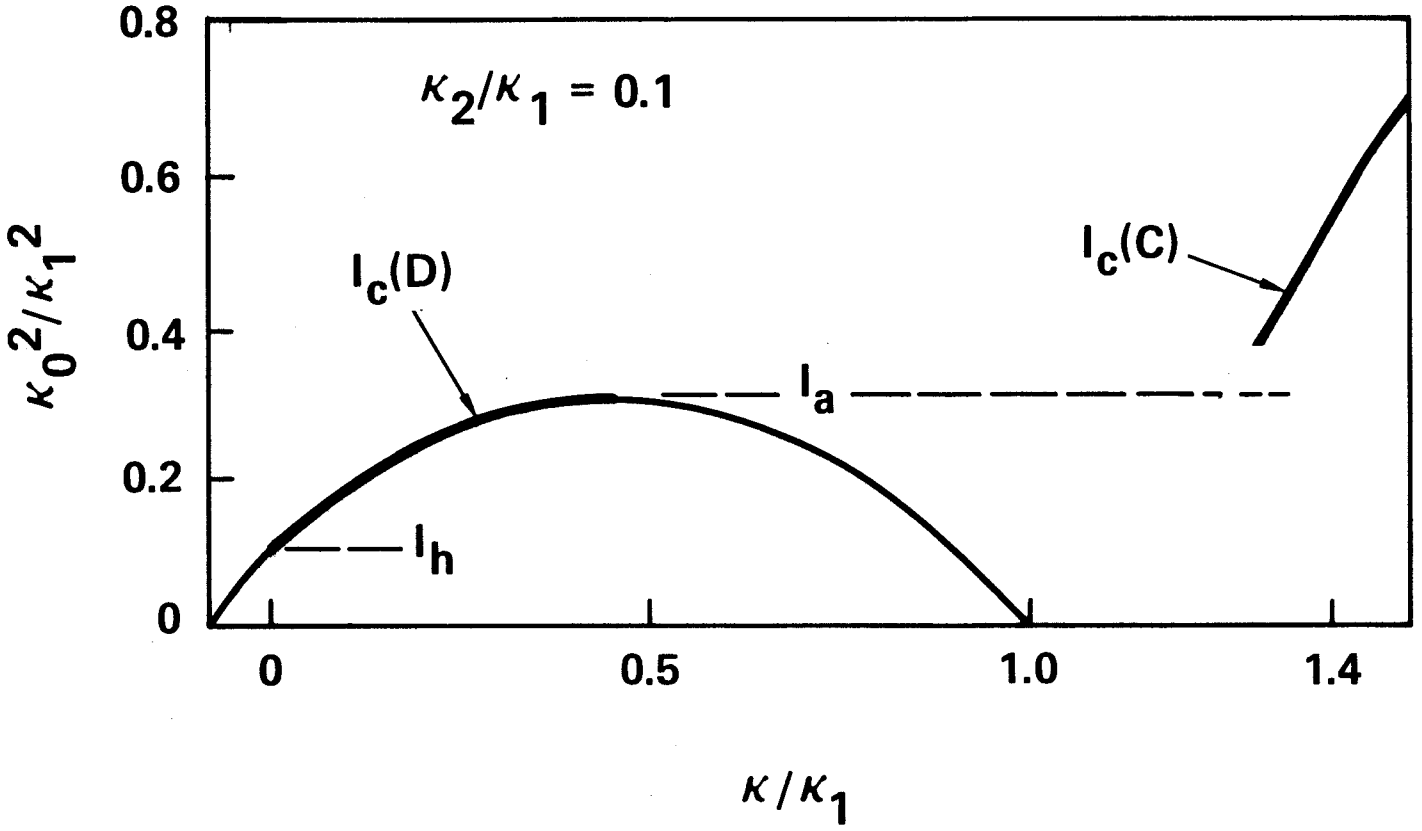
0.8
0.6
0.4
0.2
0
$\kappa_2/\kappa_1 = 0.1$
$I_c(D)$
$I_c(C)$
I_a
I_h
κ_0^2/κ_1^2
0
0.5
1.0
1.4
κ/κ_1

FIGURE 1

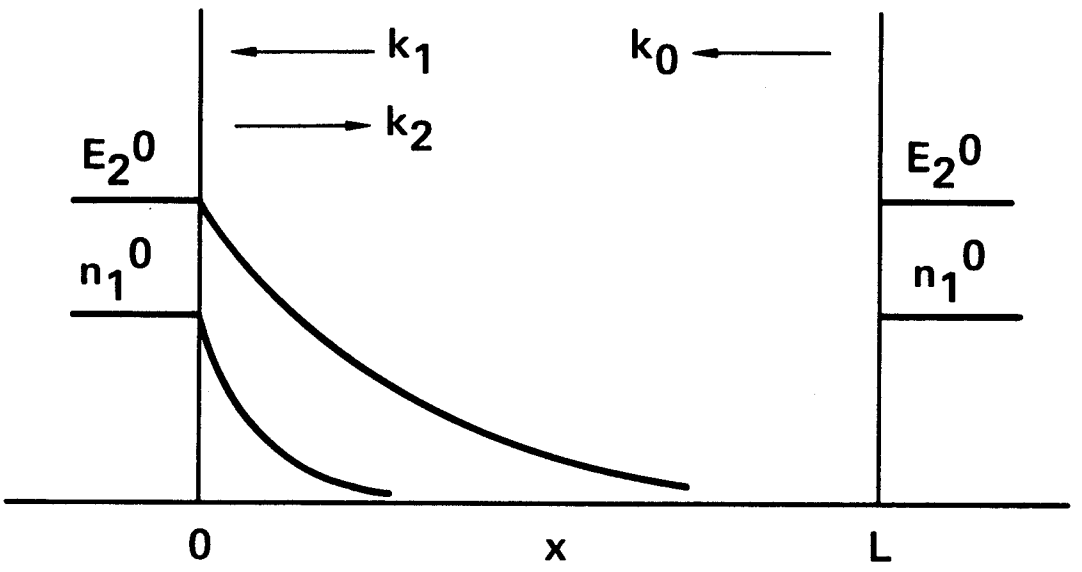

(A)

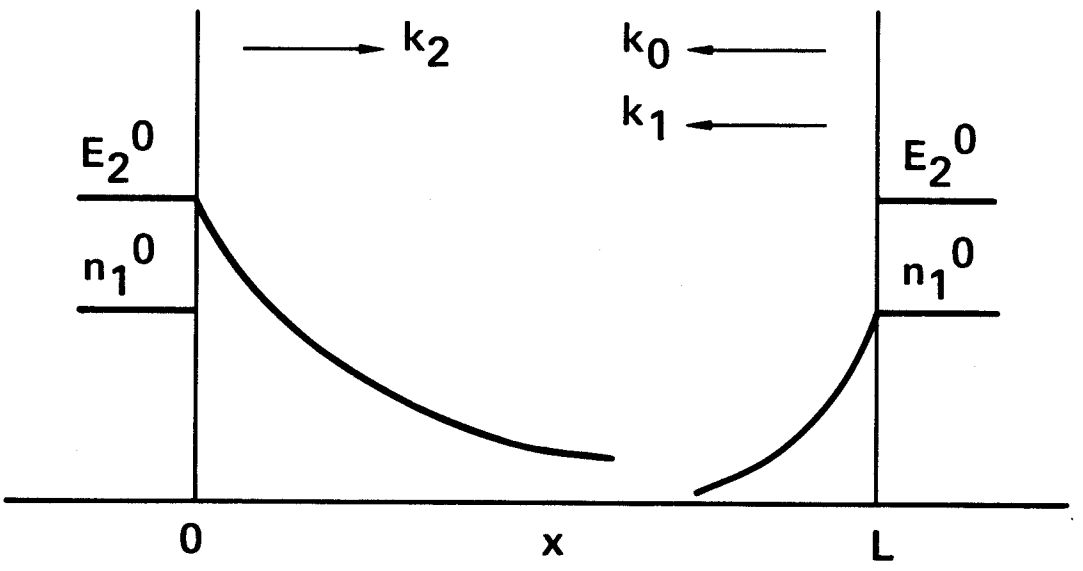

(B)

FIGURE 2

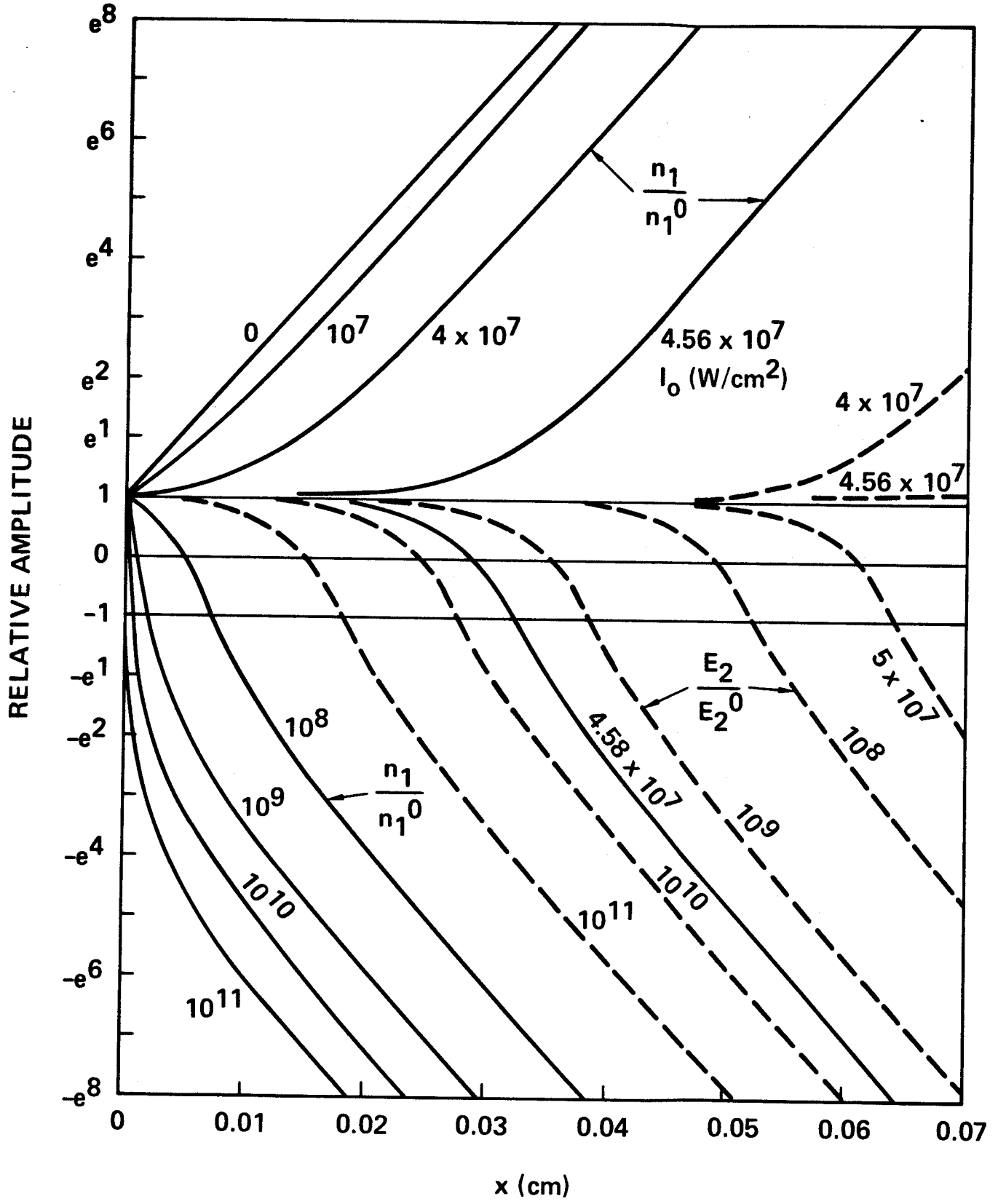
RELATIVE AMPLITUDE
e^8
e^6
e^4
e^2
e^1
1
0
-1
-e^1
-e^2
-e^4
-e^6
-e^8
0
0.01
0.02
0.03
0.04
0.05
0.06
0.07
x (cm)
n1/n1^0
0
10^7
4 x 10^7
4.56 x 10^7
I_o (W/cm^2)
4 x 10^7
4.56 x 10^7
E2/E2^0
5 x 10^7
10^8
4.58 x 10^7
10^9
10^10
10^11
n1/n1^0
10^8
10^9
10^10
10^11

FIGURE 3

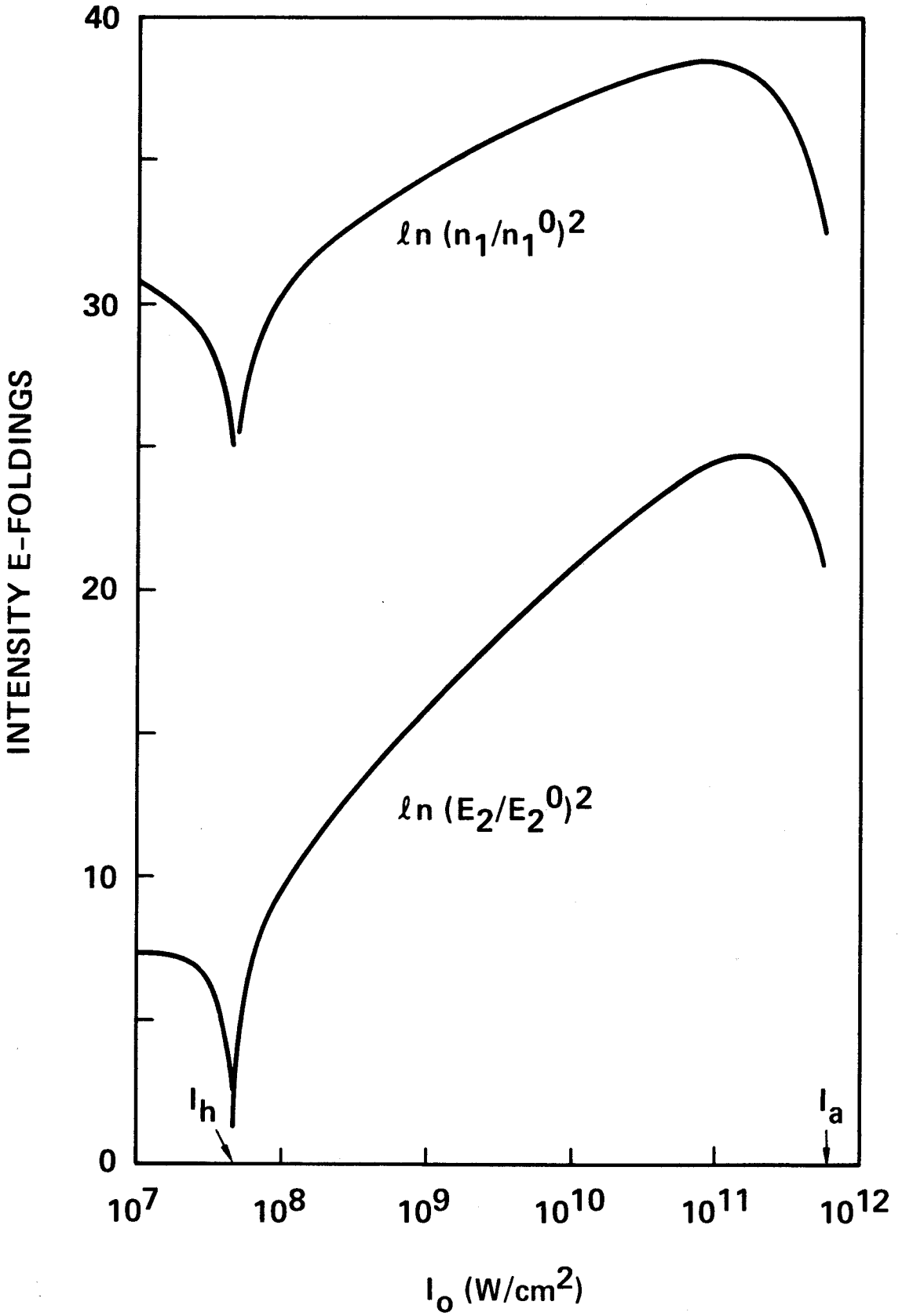
40
30
20
10
0
INTENSITY E-FOLDINGS
ℓn (n1/n1 0)2
ℓn (E2/E2 0)2
Ih
Ia
10^7
10^8
10^9
10^10
10^11
10^12
Io (W/cm2)

FIGURE 4

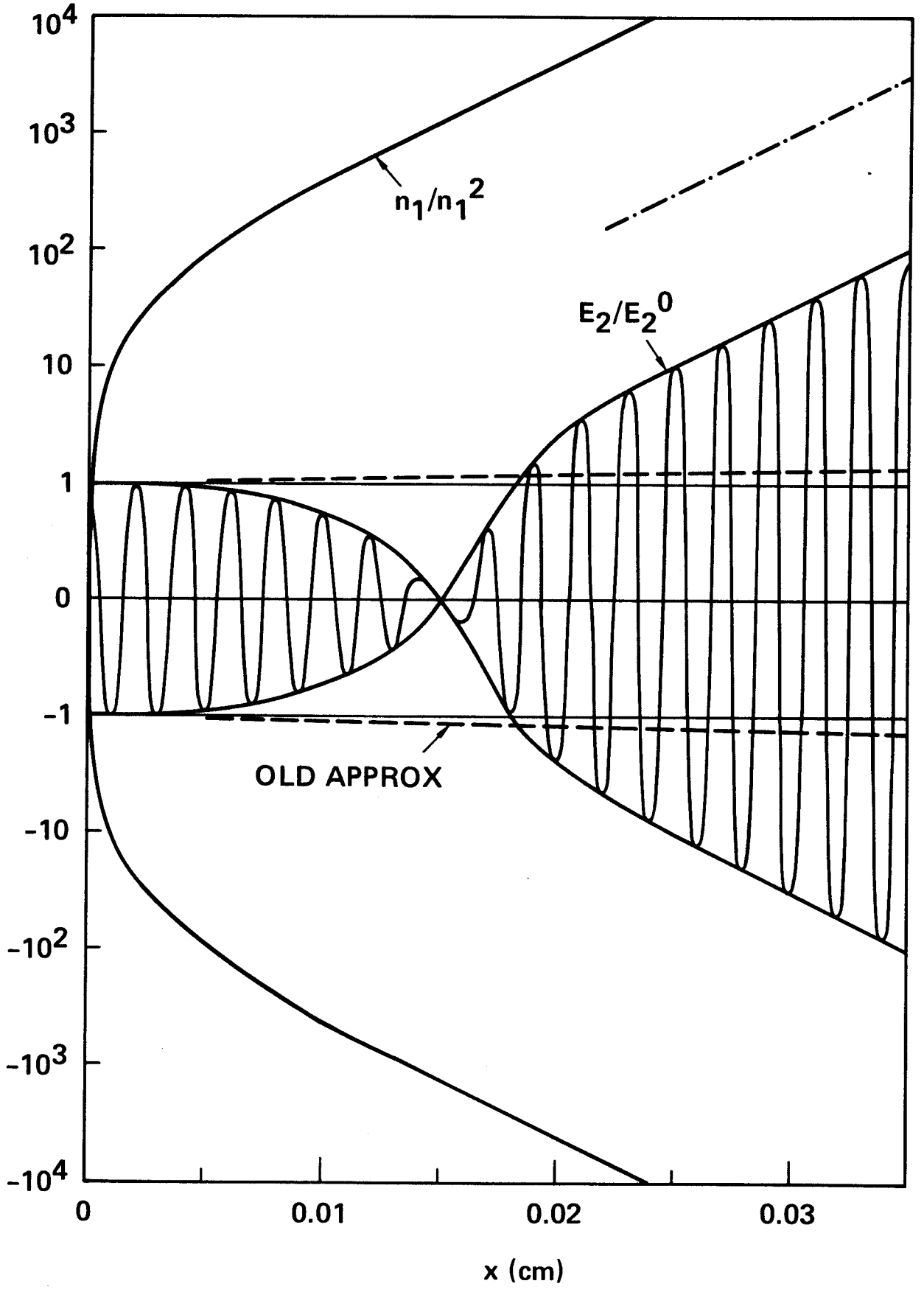
10^4
10^3
10^2
10
1
0
-1
-10
-10^2
-10^3
-10^4
n_1/n_1^2
E_2/E_2^0
OLD APPROX
0
0.01
0.02
0.03
x (cm)

FIGURE 5

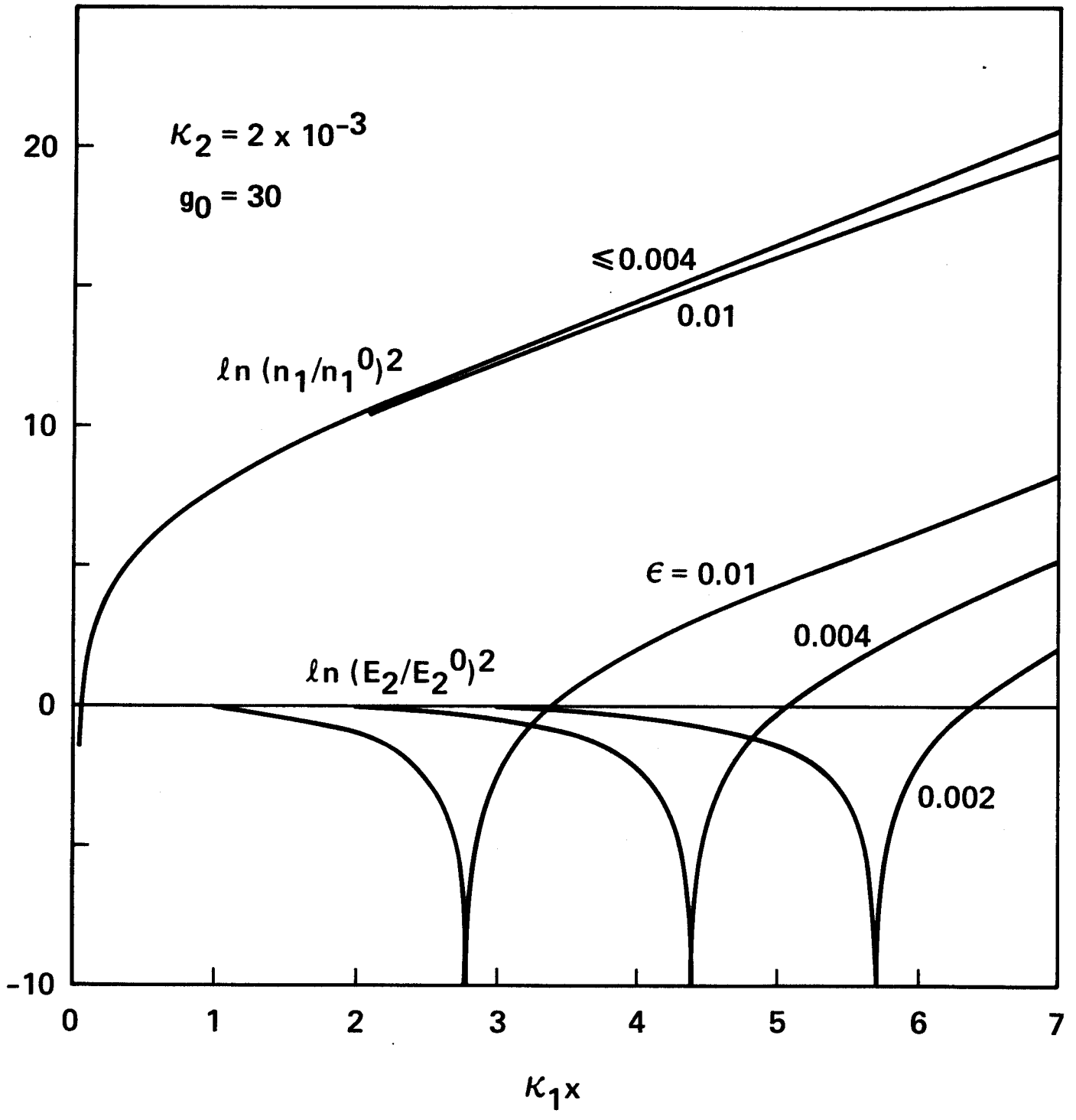
$\kappa_2 = 2 \times 10^{-3}$
$g_0 = 30$
$\leqslant 0.004$
0.01
$\ell n\,(n_1/n_1{}^0)^2$
$\epsilon = 0.01$
0.004
$\ell n\,(E_2/E_2{}^0)^2$
0.002
20
10
0
-10
0
1
2
3
4
5
6
7
$\kappa_1 x$

FIGURE 6

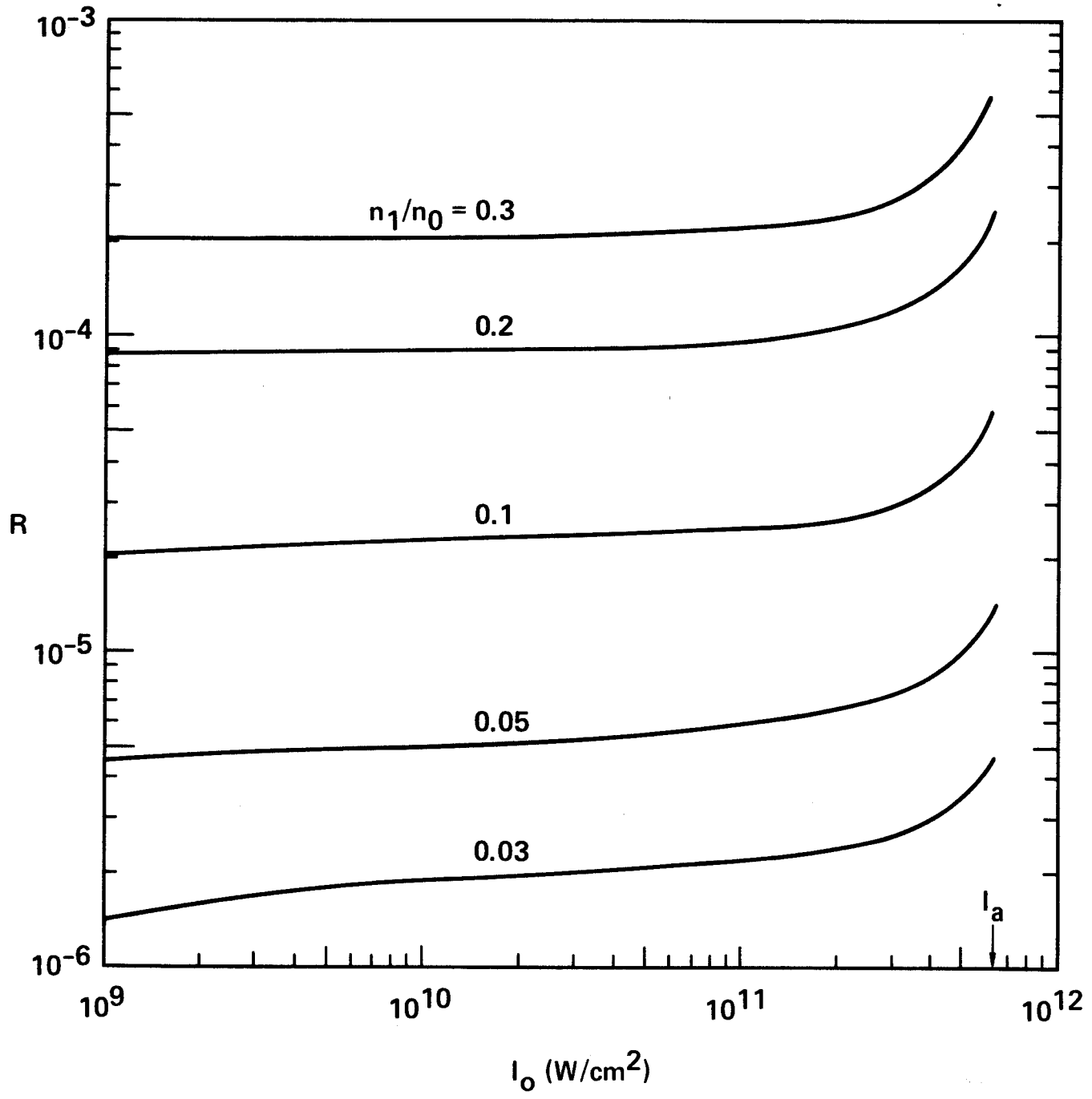
10^{-3}
10^{-4}
10^{-5}
10^{-6}
R
$n_1/n_0 = 0.3$
0.2
0.1
0.05
0.03
I_a
10^9
10^{10}
10^{11}
10^{12}
I_o (W/cm^2)

FIGURE 7

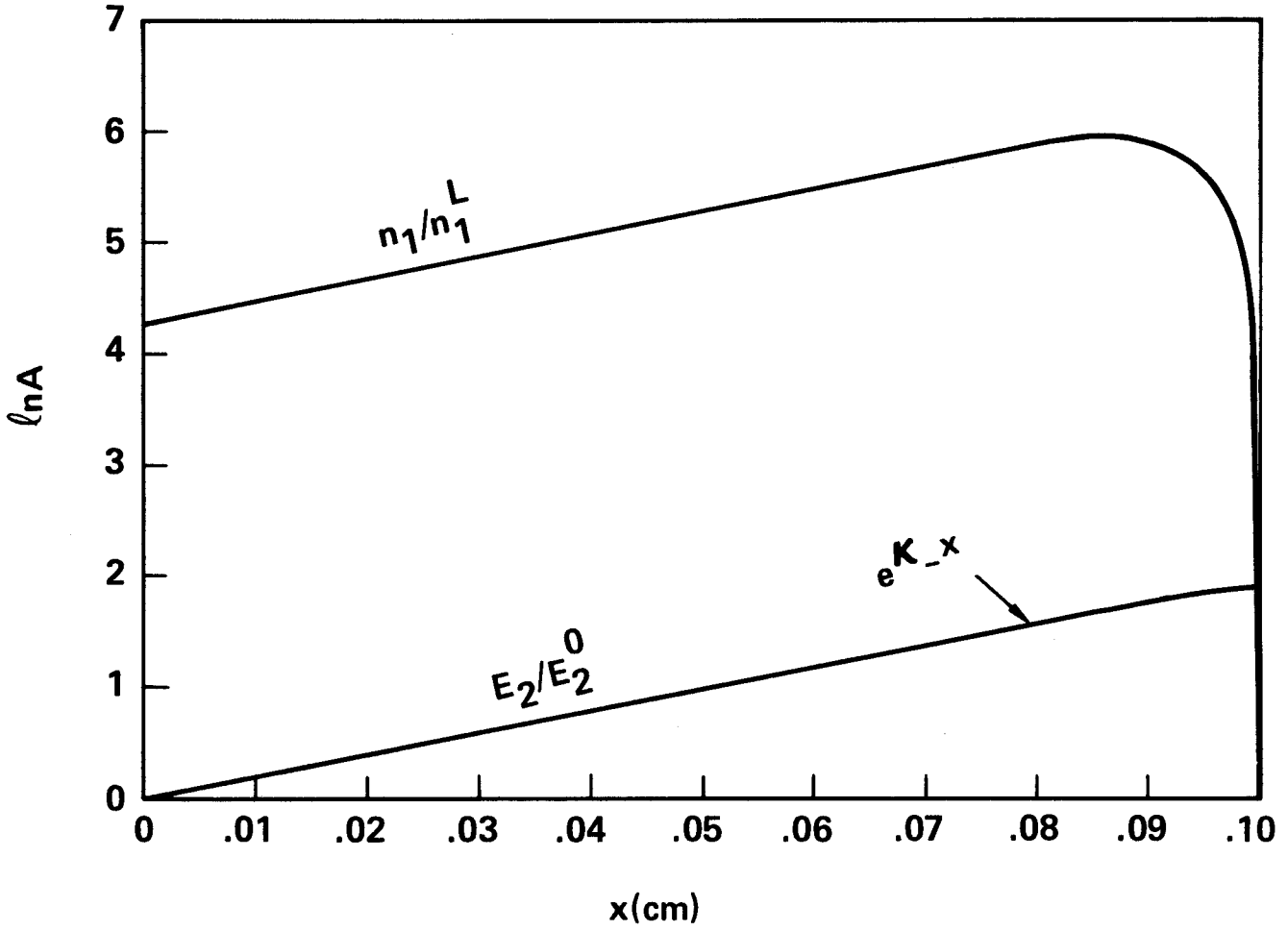

FIGURE 8

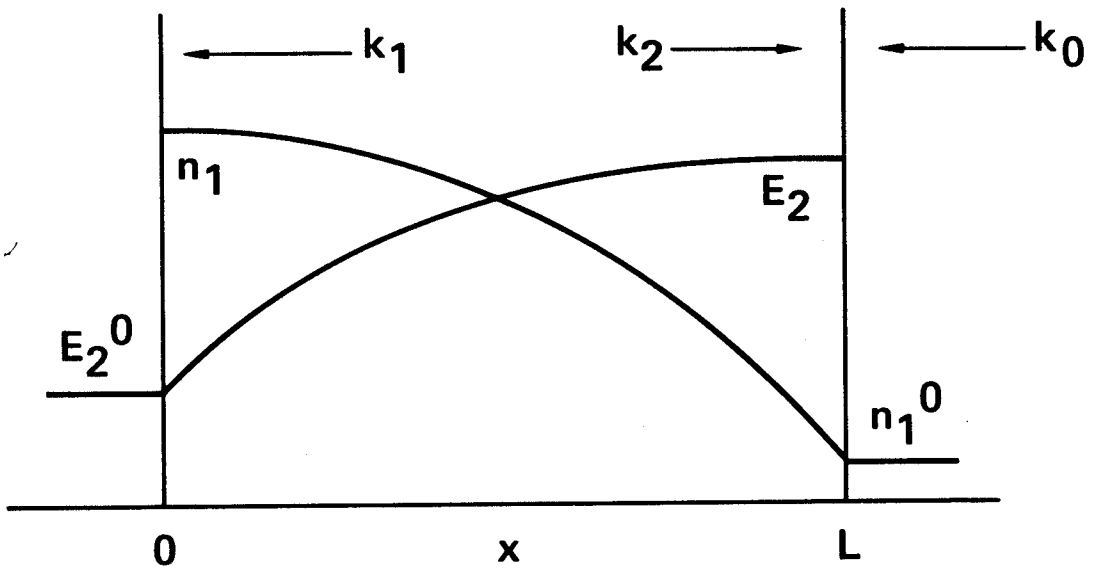

FIGURE 9

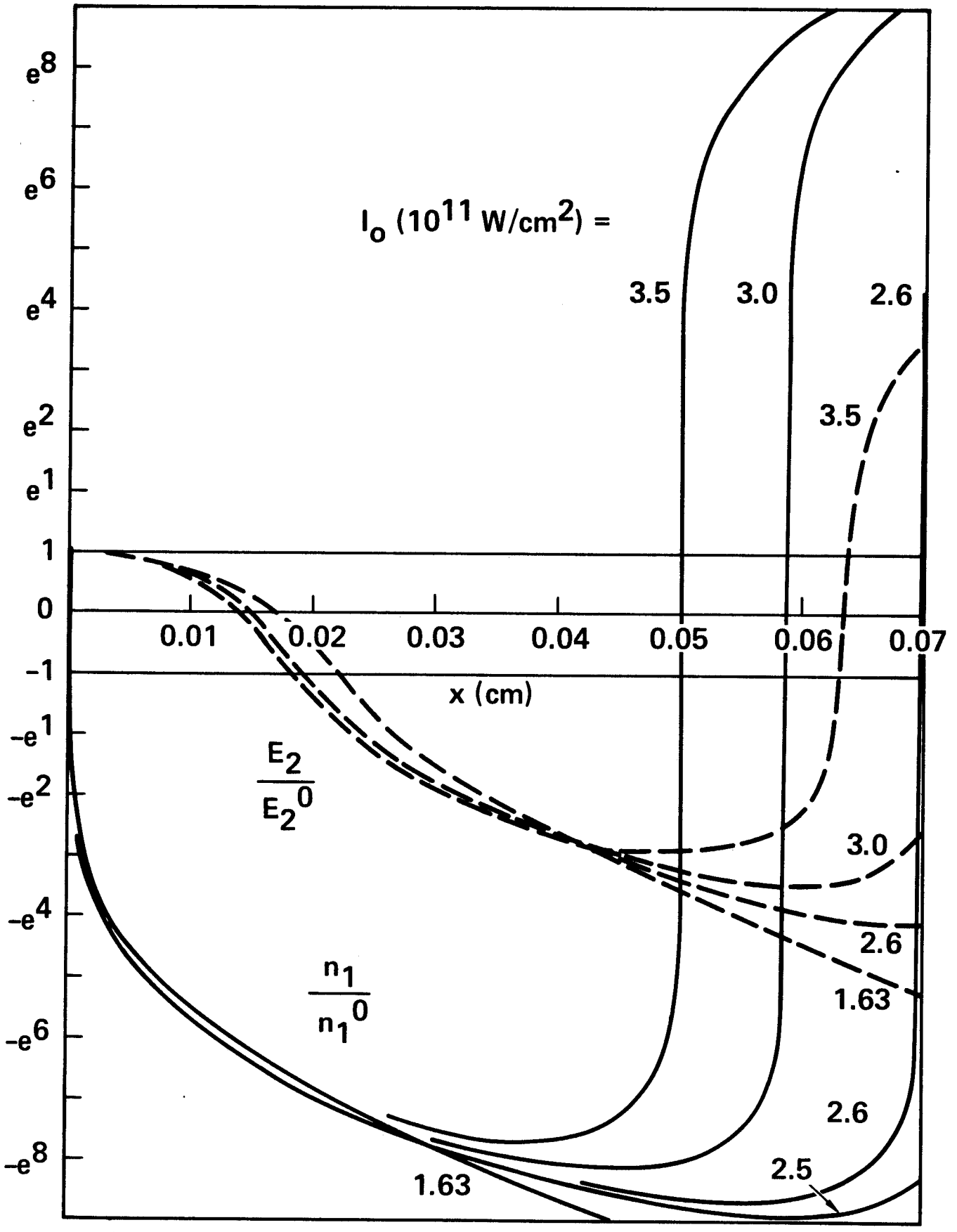
e^8
e^6
e^4
e^2
e^1
1
0
-1
$-e^1$
$-e^2$
$-e^4$
$-e^6$
$-e^8$
I_o (10^{11} W/cm^2) =
3.5
3.0
2.6
3.5
0.01
0.02
0.03
0.04
0.05
0.06
0.07
x (cm)
$\frac{E_2}{E_2^0}$
3.0
2.6
1.63
$\frac{n_1}{n_1^0}$
2.6
2.5
1.63

FIGURE 10

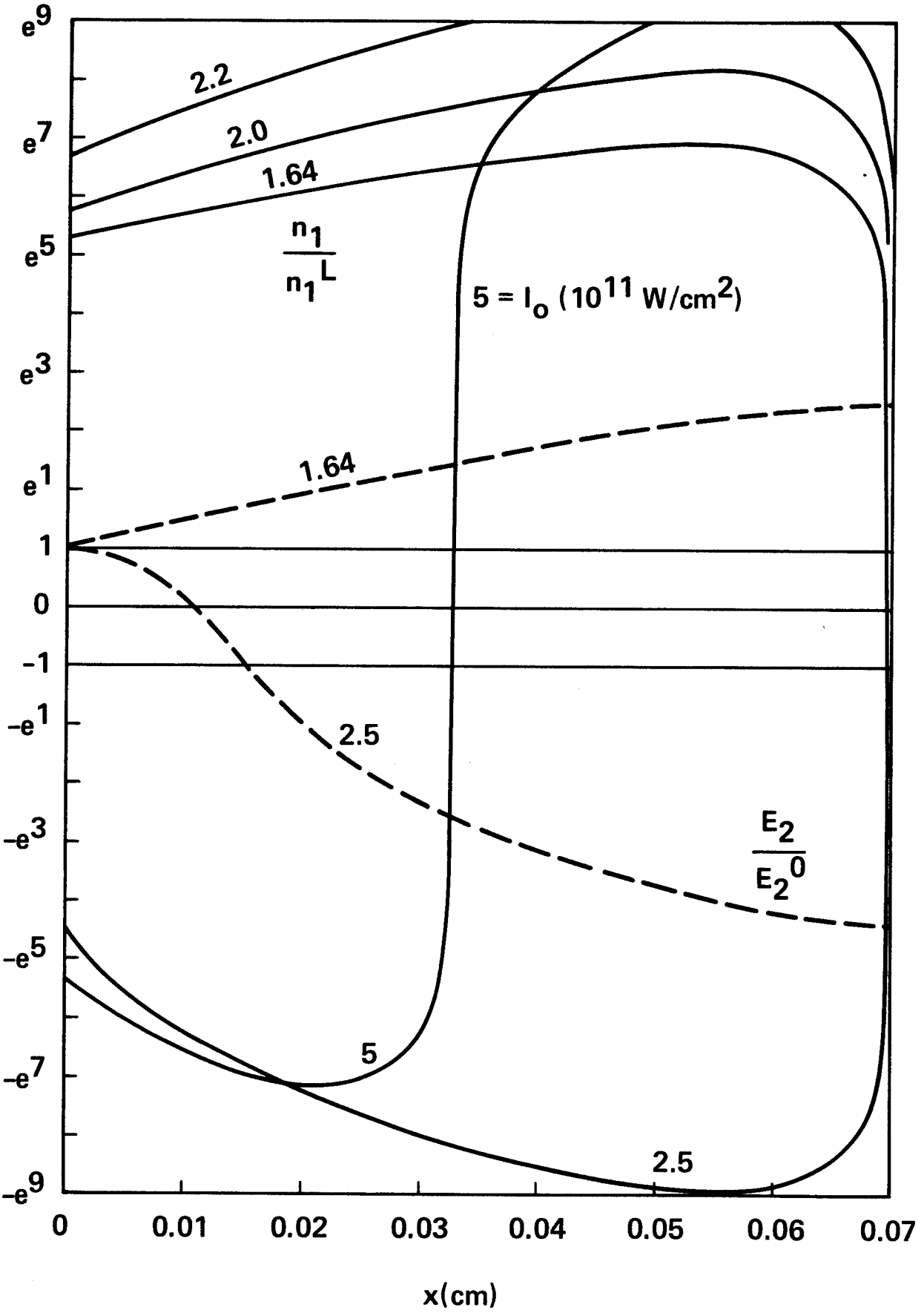
e9
e7
e5
e3
e1
1
0
-1
-e1
-e3
-e5
-e7
-e9
2.2
2.0
1.64
n1/n1L
5 = I0 (10^11 W/cm^2)
1.64
2.5
E2/E2^0
5
2.5
0
0.01
0.02
0.03
0.04
0.05
0.06
0.07
x(cm)

FIGURE 11

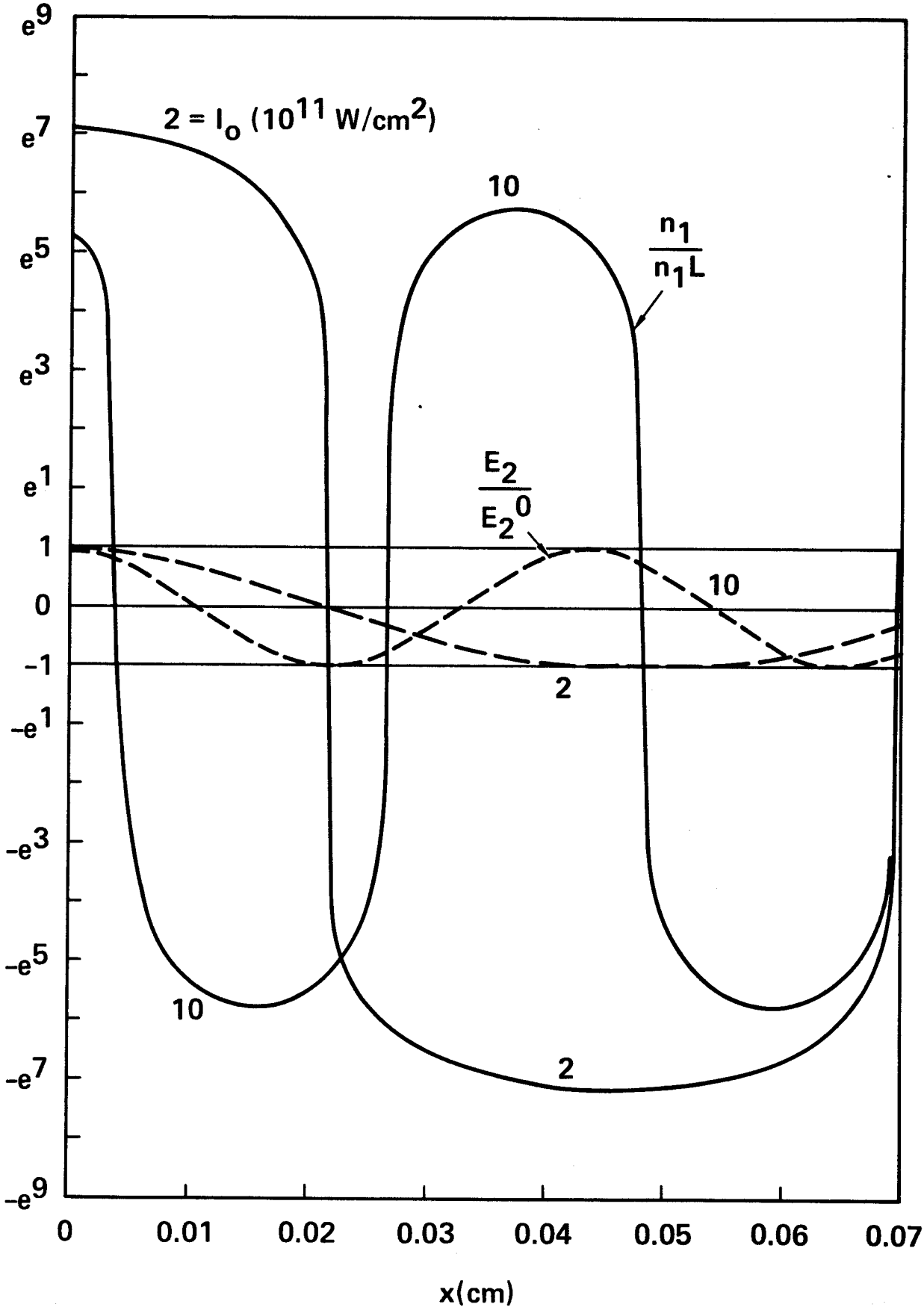
e9
e7
e5
e3
e1
1
0
-1
-e1
-e3
-e5
-e7
-e9
2 = I_o (10^11 W/cm^2)
10
n_1 / n_1L
E_2 / E_2^0
10
2
10
2
0
0.01
0.02
0.03
0.04
0.05
0.06
0.07
x(cm)

FIGURE 12

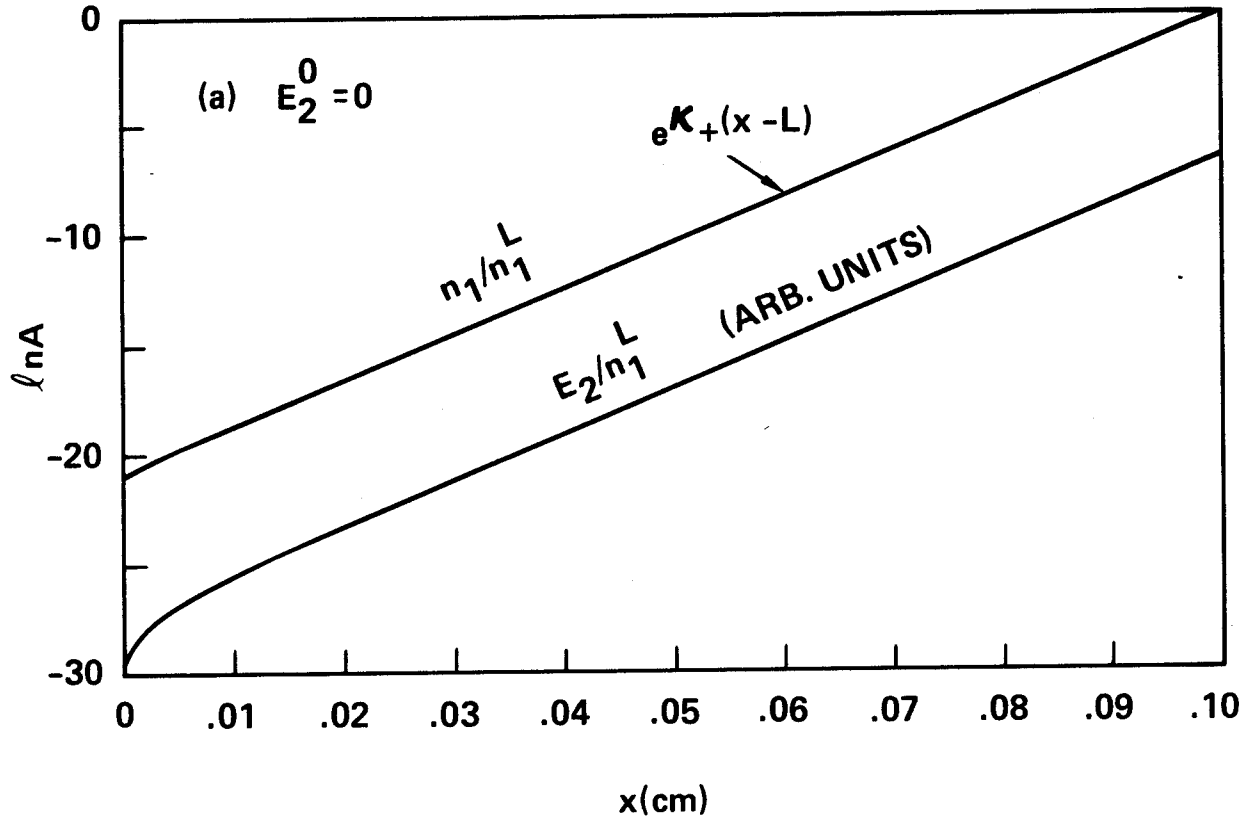
0
-10
-20
-30
ℓnA
(a) $E_2^0 = 0$
$e^{\kappa_+(x-L)}$
n_1/n_1^L
E_2/n_1^L (ARB. UNITS)
0 .01 .02 .03 .04 .05 .06 .07 .08 .09 .10
x(cm)

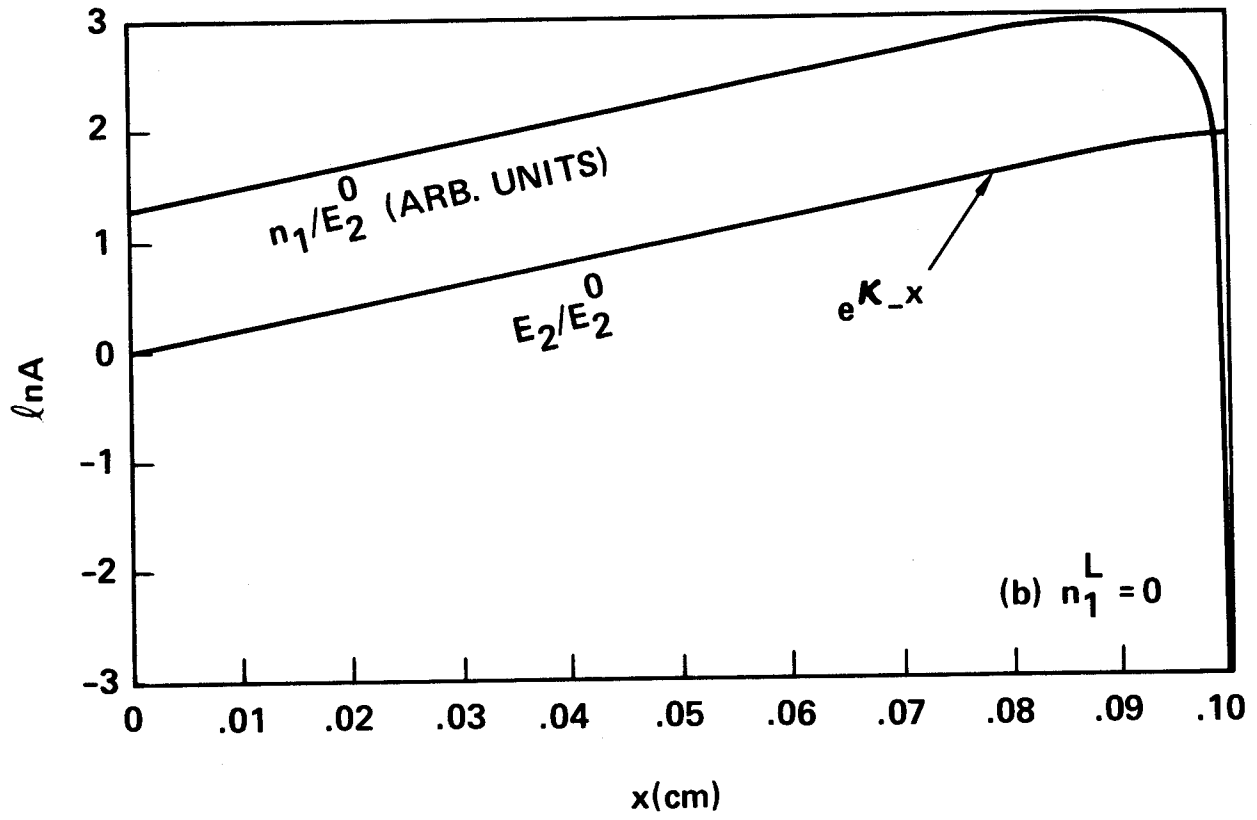
3
2
1
0
-1
-2
-3
ℓnA
n_1/E_2^0 (ARB. UNITS)
E_2/E_2^0
$e^{\kappa_- x}$
(b) $n_1^L = 0$
0 .01 .02 .03 .04 .05 .06 .07 .08 .09 .10
x(cm)

FIGURE 13

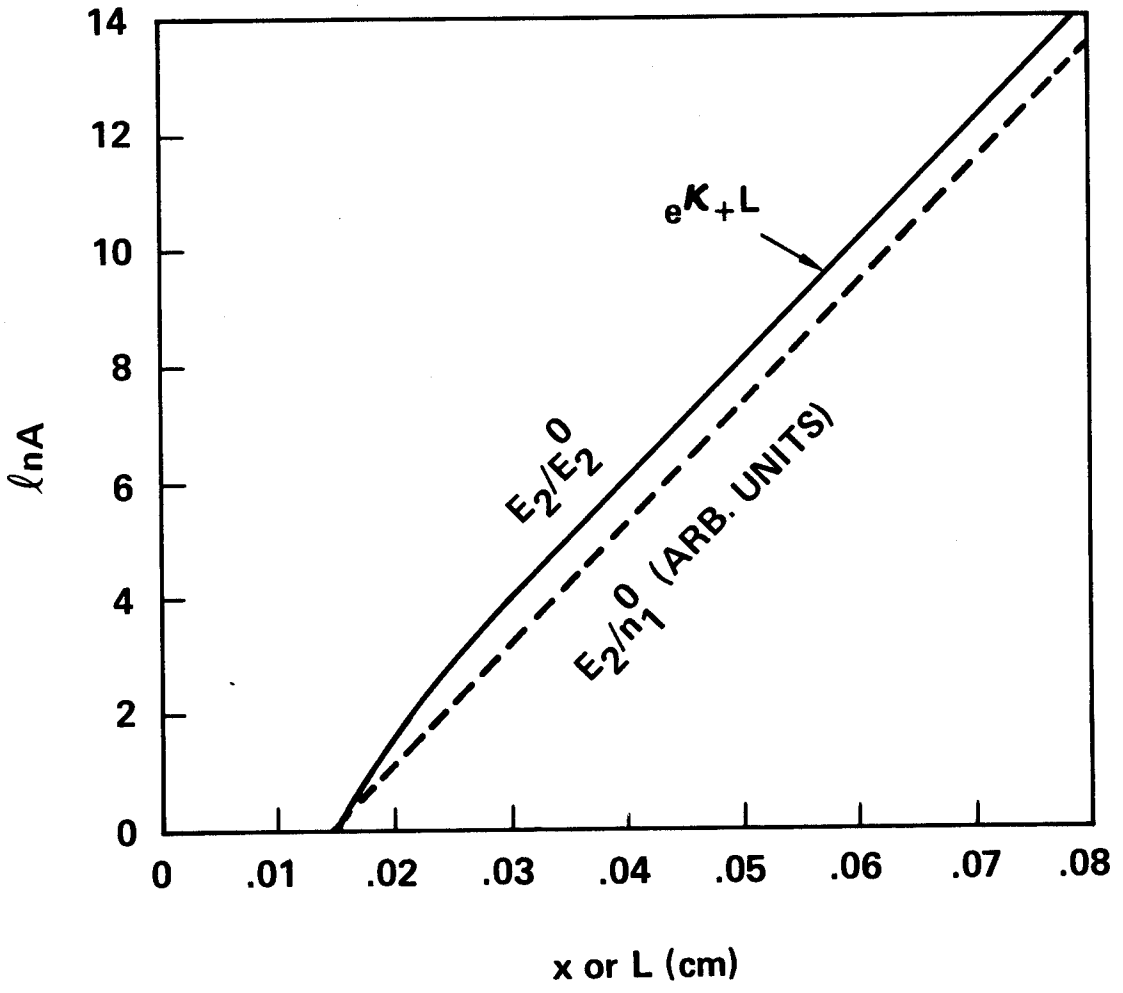
14
12
10
8
6
4
2
0
ℓnA
0
.01
.02
.03
.04
.05
.06
.07
.08
x or L (cm)
$e^{K_+ L}$
E_2/E_2^0
E_2/n_1^0 (ARB. UNITS)

FIGURE 14

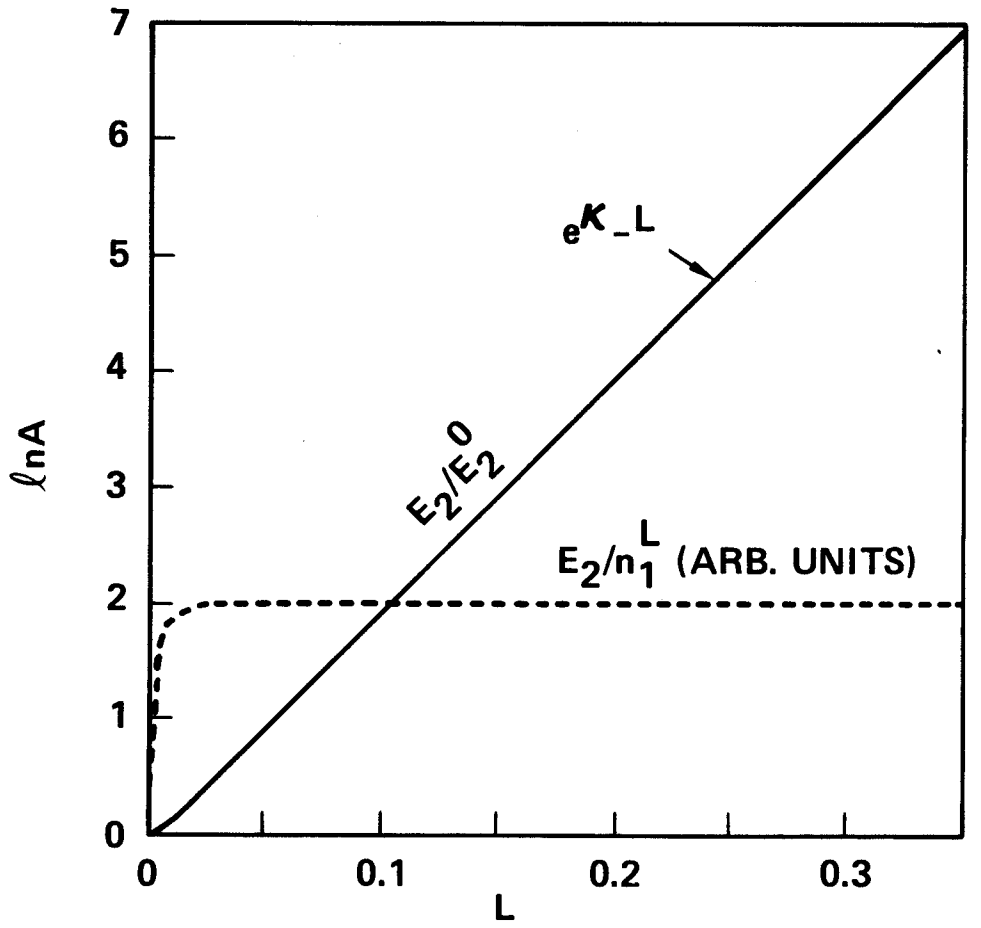

FIGURE 15